Journal of Sedimentary Research

Journal of Sedimentary Research, 2020, v. 90, 609–628
Research Article
DOI: http://dx.doi.org/10.2110/jsr.2020.32

CALCIC VERTISOLS IN THE UPPER *DAPTOCEPHALUS* ASSEMBLAGE ZONE, BALFOUR FORMATION, KAROO BASIN, SOUTH AFRICA: IMPLICATIONS FOR LATE PERMIAN CLIMATE

ROBERT A. GASTALDO,[1] KACI KUS,*[1] NEIL TABOR,[2] AND JOHANN NEVELING[3]
[1]*Department of Geology, Colby College, Waterville, Maine 04901 U.S.A.*
[2]*Department of Earth Science, Southern Methodist University, Dallas, Texas 75275, U.S.A.*
[3]*Council for Geoscience, Private Bag x112, Pretoria 001, South Africa*
e-mail: ragastal@colby.edu

ABSTRACT: **The fully continental succession of the Beaufort Group, Karoo Basin, South Africa, has been used in the development of environmental models proposed for the interval that spans the contact between the *Daptocephalus* to *Lystrosaurus* Assemblage Zones, associated by some workers with the end-Permian extinction event. An aridification trend is widely accepted, yet geochemical data indicate that the majority of *in situ* paleosols encountered in this interval developed in waterlogged environments. To date, the presence of calcic paleosols in the latest Permian can be inferred only from the presence of calcite-cemented pedogenic nodules concentrated in fluvial channel-lag deposits. Here, we report on the first empirical evidence of *in situ* calcic Vertisols found in the upper *Daptocephalus* Assemblage Zone near Old Wapadsberg Pass, one of eight classic localities in which the vertebrate turnover is reported in the Karoo Basin. Seven discrete intervals of calcic Vertisols, exposed over a very limited lateral extent, occur in an ~ 25 m stratigraphic interval. Estimates of mean annual temperature and mean annual precipitation are calculated from geochemical measurements of one paleosol, and these estimates indicate that the prevailing climate at the time of pedogenesis was seasonally cold and humid. Correlation with adjacent stratigraphic sections indicates that the late Permian landscape experienced poorly drained and better-drained phases, interpreted to reflect a climate that varied between episodically dry and episodically wet. In contrast to a paleoenvironmental reconstruction of unidirectional aridification from strata in the Wapadsberg Pass region, this study provides new evidence for a wetting trend towards the *Daptocephalus–Lystrosaurus* Assemblage-Zone boundary.**

INTRODUCTION

The stratigraphic succession in the Beaufort Group of the Karoo Basin, South Africa, is reported as a continuous record of fully continental sedimentation in which the terrestrial response to the end-Permian crisis is recorded. The turnover in vertebrate paleontology, from the *Daptocephalus* Assemblage Zone (AZ) to the *Lystrosaurus* Assemblage Zone, is considered by many (Smith 1995; Retallack et al. 2003; Ward et al. 2005; Benton and Newell 2014; Smith and Botha-Brink 2014; Viglietti et al. 2017, 2018; and others) to be coeval with the Permian–Triassic boundary events recorded in the marine realm (Shen et al. 2018), dated between 251.941 ± 0.037 and 251.880 ± 0.031 Ma (Burgess et al. 2014). The emplacement of the Siberian Traps, a Large Igneous Province (LIP) in Russia, which initiated ~ 252.20 ± 0.12 Ma and endured for less than 2 My (Burgess and Bowring 2015), released large quantities of volcanic SO_2, CO_2, and CH_4 (Maruoka et al. 2003; MacLeod et al. 2017). It is suspected that increased atmospheric greenhouse-gas concentrations resulting from this LIP event, in turn, led to a warmer atmosphere, and concomitant warming of sea-surface temperatures (Song et al. 2014; Cui and Kump 2014). Consequences of this global warming trend include expansive oceanic anoxia (Hotinski et al. 2001) and an impact on terrestrial ecosystems.

On land, warming, aridification, acid rain, shifting climatic belts, and a reduction of atmospheric oxygen concentrations are interpreted to have resulted in enhanced weathering, changes in fluvial regimes (Ward et al. 2000, 2005; Smith and Botha-Brink 2014), and wildfire (Macleod et al. 2017). Several workers (Smith and Botha-Brink 2014) assert a rapid climate shift towards aridification occurring over a short stratigraphic interval of ~ 60 meters in the Elandsburg and Palingkloof members, Balfour Formation (Fig. 1), of the main Karoo Basin in South Africa. More recently, Viglietti et al. (2018) proposed a more protracted climatic drying of an unspecified duration based on lithofacies trends. This perceived unidirectional drying trend, accompanied by increasing temperature, is thought to have culminated in an extensive, basin-wide playa-lake depositional system. This playa-lake system has been proposed to act as a unique stratigraphic datum in the basin (e.g., Smith and Ward 2001; Botha-Brink et al. 2014). That datum is equated to the transition between the *Daptocephalus–Lystrosaurus* Assemblage Zones and reportedly used for correlation between widely separated fossil sites. The utility of the proposed basin-wide playa-system stratigraphic datum has been demonstrated to be problematic and unreliable (Gastaldo et al. 2009; Gastaldo and Neveling 2016), and no empirical evidence exists to support the presence of these playa-lake deposits in the basin (Gastaldo et al. 2019a, 2019b).

* Present Address: Colorado School of Mines, Department of Geology and Geological Engineering, 1516 Illinois Street, Golden, Colorado 80401, U.S.A.

Published Online: June 2020
 1527-1404/20/090-609

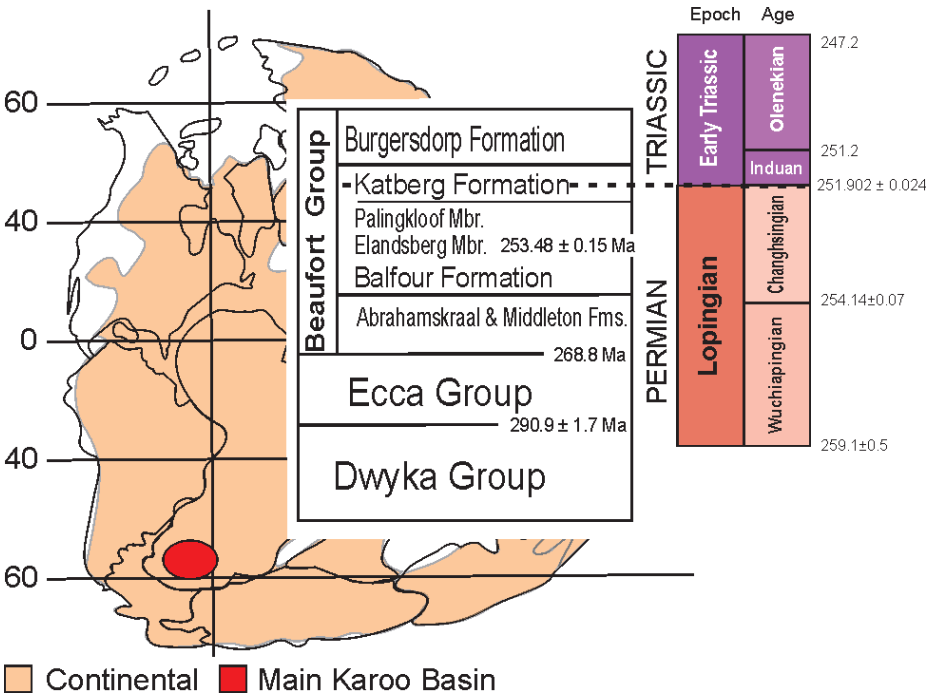

FIG. 1.—Paleogeographic map of the Late Permian (after Heydari et al. 2000) on which continental landmasses and the main Karoo Basin are located. Generalized stratigraphy of the Karoo Basin with a focus on the Upper Permian and Lower Triassic succession. Geochronometric age constraints for stage boundaries follow the International Chronostratigraphic Chart v2018/08 (www.stratigraphy.org), the age constraint on the Elandsberg Member follows Gastaldo et al. (2015, 2018), and the placement of the Permian–Triassic Boundary in the Katberg Formation follows Gastaldo et al. (2015, 2017).

The widely accepted model for the terrestrial Permian–Triassic Mass Extinction (PTME; Smith and Botha-Brink 2014; Viglietti et al. 2017, 2018) in the Main Karoo Basin uses sedimentologic, taphonomic, and geochemical observations to posit a unidirectional climatic drying trend across the assemblage-zone boundary, the magnitude of which was sufficient to induce a recognizable ecosystem disruption (Roopnarine et al. 2017). This climatic shift is associated with the first occurrence of mudrock reddening (rubification) and basin-wide alteration of the dominant fluvial regimes (Ward et al. 2005; Smith and Botha-Brink 2014). A reported change, from a meandering to a braided channel system, is believed to occur at or very near the Permian–Triassic system boundary throughout the Main Karoo Basin. Support for the proposed shift towards a drier and more arid climate is based on the reportedly massive nature of the overlying reddish-gray mudrock Facies D of Smith and Botha-Brink (2014). This reddening has been attributed to an increased iron-oxide component resulting from an increased eolian contribution of airborne detrital grains deposited in arid soils near the assemblage-zone boundary (Smith and Botha 2005; Smith and Botha-Brink 2014; but see Sheldon 2005; Li et al. 2017; Gastaldo et al. 2018). Increasing aridity over the interval is also interpreted from stable-isotope $\delta^{18}O$ data from apatite of dicynodont teeth and bone (MacLeod et al. 2000, 2017; Rey et al. 2016). Yet, to date, the only physical evidence for the presence of dryland or calcic paleosols in either the uppermost Balfour or lowermost Katberg formations, which would confirm a unidirectional trend, are pedogenic nodule conglomeratic lag deposits and soil aggregates concentrated at the bases of fluvial channels (Pace et al. 2009; Gastaldo et al. 2013, 2018).

The investigation of paleosol profiles is a common approach to paleoenvironmental and paleoclimatic reconstruction from continental and mixed marine-and-continental strata through the Phanerozoic. In fact, many recent studies have sought to assemble large volumes of observations and measurements from numerous paleosols contained in thick stratigraphic successions (e.g., Krauss 1987, 1997; Tabor and Montañez 2004) or along basin-wide transects (Bown and Krauss 1987; Rosenau et al. 2013a, 2013b). Yet, the study of paleosols has its origins associated with detailed studies of individual profiles to ascertain specific soil-forming processes and mechanisms that are important for paleoenvironmental reconstructions (e.g., Abbott et al. 1976). This detailed approach has remained a mainstay for many recent studies of paleosols and actualistic studies of modern soils (Wright and Wilson 1987; Retallack and German-Heins 1994; Caudill et al. 1996, 2008; Gill and Yemane 1996; Capo et al. 2000; Driese et al. 2000). This practice of focused study on individual paleosol profiles is especially common in geochemical, proxy-based investigations due, in large part, to the time- and resource-intensive nature of these investigations (e.g., Hsieh and Yapp 1999; Vitali et al. 2002; Yapp 2004; Tabor et al. 2004a, 2004b; Tabor and Yapp 2005; Feng and Yapp 2009; Gulbranson et al. 2011). The Karoo Basin is no exception in this regard (Gastaldo et al. 2014). Herein, we extend upon previous detailed studies of individual profiles via geochemical analysis of a calcareous paleosol from the upper *Daptocephalus* Assemblage Zone near Old Wapadsberg Pass, one of eight classic localities in which the vertebrate turnover is reported in the Karoo Basin. This paleosol is one of seven pedogenically altered stratigraphic layers that occur more than 100 m below the *Daptocephalus–Lystrosaurus* vertebrate assemblage-zone boundary. Hence, these represent depositional settings older than the beginning of the previously interpreted, rapid climatic drying trend described in Smith and Botha-Brink (2014). We assess the geochemical weathering trends of the lowermost paleosol profile in the 527/Quaggasfontein stratigraphic section to evaluate the environmental and climatic conditions of its formation and, by proxy, place constraints on the conditions under which the similarly organized six other profiles developed in the latest Permian *Daptocephalus* zone of the Main Karoo Basin.

GEOLOGIC SETTING

The rocks of the current study are a part of the Karoo Supergroup (Fig. 1), which ranges in age from Late Carboniferous to Middle Jurassic (Johnson et al. 2006). The Karoo Basin is, generally, interpreted as either as a retro-arc foreland basin (Catuneau et al. 2005) or a foreland basin (Viglietti et al. 2017) in which continental sediment accumulated as a consequence of mountain building associated with the subduction of the oceanic paleo-Pacific plate beneath the Gondwanan plate. In contrast, Lindeque et al. (2011) interpret the Karoo Basin as having formed ahead of

a thin-skinned Jura-type fold belt. Regardless, the formation of the Cape Fold Belt along the southern margin of the Karoo Basin acted as the provenance for its sedimentary record, and the stratigraphic succession preserves, in part, depositional systems resulting from the termination of the Late Paleozoic Ice Age. Once the southwestern half of the Gondwanan supercontinent began drifting in the Permo–Carboniferous (~ 300 Ma; Smith et al. 1993), the early Permian ice sheet receded (Isbell et al. 2008) impacting the deposition of the Karoo Supergroup for the next ~100 million years (Smith et al. 1993).

Both glacial or deglacial and alpine-derived detrital-clastic sediments constitute the basin fill. Sediments transported and deposited as a consequence of deglaciation overlie Precambrian basement rock. These are the Dwyka and Ecca groups, which represent post-glacial deltaic and turbidite deposits, respectively (Fig. 1). This glacial succession is overlain by the Beaufort Group, which is dominated by aggradational floodplain deposits (Smith et al. 1993) and subdivided into the Abrahamskraal, Middleton, Balfour, Katberg, and Burgersdorp formations (Fig. 1). Due to the homogeneity of lithologies and, until recently, a dearth of geochronometric or paleomagnetic data on which to subdivide the succession, changes in vertebrate biostratigraphy have been used to correlate deposits across the basin (Rubidge 1995, 2005). The upper member of the Balfour Formation, the Palingkloof Member, is reported to span the vertebrate-defined Permian–Triassic Boundary (PTB), whereas the overlying Katberg Formation is considered Lower Triassic (Fig. 1; Smith and Botha-Brink 2014). This assumption conforms to a paradigm first proposed by Broom (1906, 1911) that the *Dicynodon* (*Daptocephalus*; Vigletti et al. 2016) fauna is of Permian age and the overlying *Lystrosaurus* fauna is lowermost Triassic.

LOCALITY AND METHODS

The stratigraphic succession near Wapdasberg Pass in the Eastern Cape Province, South Africa, was measured using standard field techniques as described elsewhere (e.g., Gastaldo et al. 2018, 2019a, 2019b). The primary section (Fig. 2) traversed an erosional gully (donga) beginning on the border of farm 527, which today forms part of the farm Quaggasfontein, continuing to the east onto Farm 80 and Zeekoegat 77, today incorporated into the farm Pienaarsbaken (see supplemental Fig. 1). The base of the section, which is referred to as the 527/Quaggasfontein section, lies ~ 1.25 km northwest of Old Wapadsberg Pass (now abandoned) and ~ 1.9 km northwest of New Wapadsberg Pass (NWP), which was created with the construction of the R61 highway (Ward et al. 2000; Gastaldo et al. 2005; Prevec et al. 2010) (Fig. 2). Here, the main 170-m-long 527/Quagasfontein section begins at S31.909494°, E024.888792° and ends at S31.91058°, E024.90523° (Figs. 2, 3). No detailed stratigraphic section is published for the succession between Old Wapadsberg Pass and Lootsberg Pass (seven kilometers to the north), to date. A *Dicynodon laceriteps* lower jaw bone (RS 169), near the base of the 527/Quaggasfontein section, is reported in Smith and Botha-Brink (2014, Supplemental Table 1) to lie 52 m below that study's vertebrate-defined PTB at Old Wapadsberg Pass. Measured stratigraphic sections in the area are correlated using laterally continuous, resistant sandstone benches as inter-locality datums following the practice of Gastaldo et al. (2017, 2018, 2019b).

Seven discrete intervals of calcic Vertisols, encompassing a total of ~ 25 m of a siltstone-dominated part of the stratigraphic section, are identified along the donga wall (S31.90888°, E24.89065°; Figs. 2–5). Laterally equivalent and adjacent beds exposed in the same donga are very fine-grained, yellow-gray wackestone, and total > 12.5 m in thickness (Fig. 3). Hence, the calcic paleosols are not preserved, but eroded out and back-filled in the Late Permian, just a very short lateral distance southeastward from the hillside which preserves the succession with calcic paleosols. A 1.3 m interval spanning the lowermost calcareous paleosols was sampled every 10 cm in a descending stratigraphic order and labeled successively 280517.1 through 280517.14 (Fig. 4) for lithologic, petrographic, and geochemical analyses. Twelve thin sections (280517.1–280518.14) were prepared by Applied Petrographic Services in Greensburg, Pennsylvania; samples 280517.2, 280517.3, and 280517.9 were incompetent and no thin sections were prepared for analysis. Standard petrographic descriptions of lithologies were applied to all thin sections, whereas soil textural and fabric descriptions (Brewer 1964) were applied to features particular to pedogenic processes.

Geochemistry

Fourteen bulk-rock and eleven matching billets from thin-section samples from the calcic Vertisol interval were powdered using a ball mill and sent to ALS Global, Reno, Nevada, for a full-digestion analysis. There, samples underwent lithium-borate fusion prior to acid dissolution, and resulting solutes were analyzed using inductively coupled plasma-mass spectrometry (ICP-AES and ICP-MS (zircon)) to determine concentrations of selected major and minor elements. Results from ICP-MS analyses are presented in Supplemental Data Table 1.

All samples were powdered from bulk rock, reacted with 10% HCl solution to remove carbonates and other labile compounds, and rinsed with deionized water. These acid-treated powders were used to determine weight-percent total organic carbon (%TOC) and total organic nitrogen (%TON) using a Perkin Elmer 2400 Series II CHNS/O elemental analyzer housed at Colby College. Samples were analyzed in triplicate to obtain average %TOC and %TON values. Values are reported against measurements of an acetanilide standard (C = 71.09%, H = 6.71%, N = 10.36%, O = 11.84%), an aliquot of which was analyzed between every nine bulk-rock powder samples, to ensure data integrity and reproducibility. The percent total carbon loss-on-ignition (%LOI) was measured at ALS Global where one gram of powdered material for each sample was weighed, heated to 1000° C for one hour, cooled, and then reweighed. The %LOI was calculated from the difference in weight and does not discriminate between organic and carbonate forms of carbon. To calculate percent total inorganic carbon (%TIC), %TOC was subtracted from %LOI values.

Molecular weathering ratios, including base loss, clayeyness, mineral assemblage stability (MAS), calcification, salinization, and the chemical index of alteration minus potassium (CIA-K), are calculated from results of ICP-MS analyses and are plotted versus profile depth following Sheldon and Tabor (2009). These weathering ratios are calculated using the weight-percent values of all major elements, on an oxide basis, after conversion to molar abundance values. Base loss refers to the leaching of major "base" elements (Na, Ca, K, and Mg) relative to an immobile soil element (in this instance, Ti). Clayeyness is a proxy of Al relative to Si in the soil, and serves as a proxy for differential clay-mineral accumulation and composition in a weathering profile. Mineral-assemblage stability (MAS) is the ratio of Fe (recalcitrant element) to K (labile element) and serves as a proxy for breakdown and leaching of base-bearing minerals *via* hydrolytic reactions (e.g., granite weathering to oxides + kaolinite). Calcification ([Ca+Mg]/Al) and salinization ([K+Na]/Al), respectively, are proxies for the accumulation of calcium and salts in a soil profile. CIA-K values are calculated using the following equation:

$$\mathrm{CIA-K} = \mathrm{Al_2O_3}/(\mathrm{Al_2O_3} + \mathrm{CaO} + \mathrm{Na_2O}) \times 100, \quad (1)$$

whereas CALMAG (Nordt and Driese 2010) values are calculated using the following equation:

$$\mathrm{CALMAG} = \mathrm{Al_2O_3}/(\mathrm{Al_2O_3} + \mathrm{CaO} + \mathrm{MgO}) \times 100. \quad (2)$$

Bulk-rock geochemical data also were evaluated using a mass-balance approach, following Brimhall et al. (1988, 1991a, 1991b). This approach evaluates chemical variations in a soil due to: 1) the closed-system effects

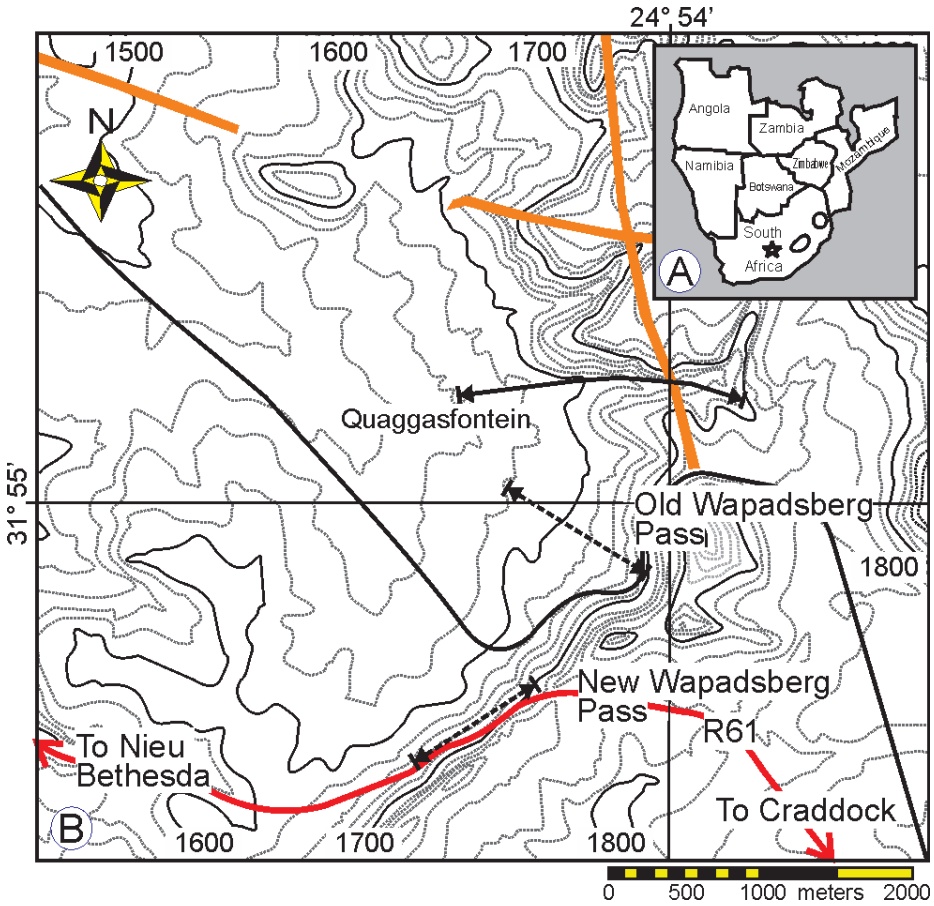

FIG. 2.—Locality maps of the study area. **A)** Generalized map of southern Africa where the star marks the site in the Eastern Cape Province. **B)** Topographic map on which New Wapadsberg Pass (NWP) lies on the blacktop R61 highway, Old Wapadsberg Pass (OWP) is located to the north constructed as a gravel-and-dirt roadway, with the section measured along a donga oriented at right angles to it. The base of the 527/Quaggasfontein stratigraphic section with Vertisols begins ~ 1.25 km to the northwest on the farm 527/Quaggasfontein and continues onto the farm Pienaarsbaken (solid black line with arrows). Gastaldo et al. (2014, supplemental data) published measured stratigraphic sections from both NWP and OWP, both of which are shown as dashed lines with arrows. Surficially exposed dolerite dikes are shown in orange. Contour interval is 20 m; scale in meters.

of residual enrichment and volumetric changes in the soil matrix, and 2) open-system transport of material into or out of the soil (Driese et al. 2000). Mass-balance relationships account for changes in parent material (protolith) as a result of pedogenesis. Typically, a sample of the C horizon is collected and used as representative parent material. Mass-balance graphs for carbonate leaching, redoximorphy, biocycling, and clay accumulation are plotted versus profile depth following Driese et al. (2000). Mass-balance calculations are made with Ti as the immobile element using materials taken from the interpreted C horizon of the Quaggasfontein paleosol profile, at a depth 110–120 cm (Figs. 3, 4; Supplemental Data Table 2). Carbonate leaching, redoximorphy, and biocycling and clay accumulation measures the enrichment or depletion of Ca and Mg, Mn and Fe, P, and Na+K+Al+Si, respectively, through the soil profile.

Mass-balance calculations are made following Driese et al. (2000) using the following equations:

$$\varepsilon_{i,w} = \frac{\rho_p C_{ip}}{\rho_w C_{iw}} - 1 \quad (3)$$

where ε is the strain (volumetric change) of the weathered material; *i* is an immobile index element, such as Ti or Zr, in the weathered material (*w*); ρ_p and ρ_w are the bulk densities of the parent and weathered material, respectively; and $C_{i,p}$ and $C_{i,w}$ are the concentrations of immobile element *i*, in the parent and weathered material, respectively. Strain ($\varepsilon_{i,w}$) is used to calculate the mass fraction of a chemical constituent that has been gained or lost in open-system transport. Mass transport ($t_{j,w}$) of a constituent, *j*, in the weathered material is calculated by

$$\tau_{i,w} = \left(\frac{\rho_w C_{j,w}}{\rho_p C_{j,p}}\right)(\varepsilon_{j,p}) - 1 \quad (4)$$

where terms are described as above and in Driese et al. (2000). The bulk density of the paleosols is a factor in the calculation of strain (the positive or negative volumetric changes; Driese et al. 2000) and translocation of elements in the paleosol. The bulk densities of the fourteen samples down the profile were not measured; hence, all mass balance calculations were made under the assumption that the bulk densities of all samples were 2.2 g/cm^2 (S. Driese, personal communication, 25 November 2017).

Calcite-cemented nodules of various diameters were collected from four horizons in the lower Quaggasfontein paleosol profile (Figs. 3, 5). These were cut at Southern Methodist University, described, and analyzed for stable carbon- and oxygen-isotope analysis, following Gastaldo et al. (2014). Micrite and microspar cement samples were drilled from nodules or polished matching billets from thin sections using an x, y, z drill mount. Sample powders were reacted with 100% orthophosphoric acid at 25° C *in-vacuo*, under closed-system conditions, to produce CO_2 (McCrea 1950). CO_2 gas was cryogenically purified and analyzed for stable carbon- and oxygen-isotope compositions using an Finnigan MAT 252 isotope-ratio mass spectrometer housed in the Department of Earth Sciences at SMU.

Stable-isotope measurements are made in delta values and are reported in per mil notation:

$$\delta^{13}C \text{ (or } \delta^{18}O) = \left(R_{sample}/R_{standard} - 1\right) * 1000 \quad (5)$$

where $R = {}^{13}C/{}^{12}C$ and ${}^{18}O/{}^{16}O$ for carbon and oxygen, respectively. The standards used to report isotope values of calcite are an in-house Carrera-

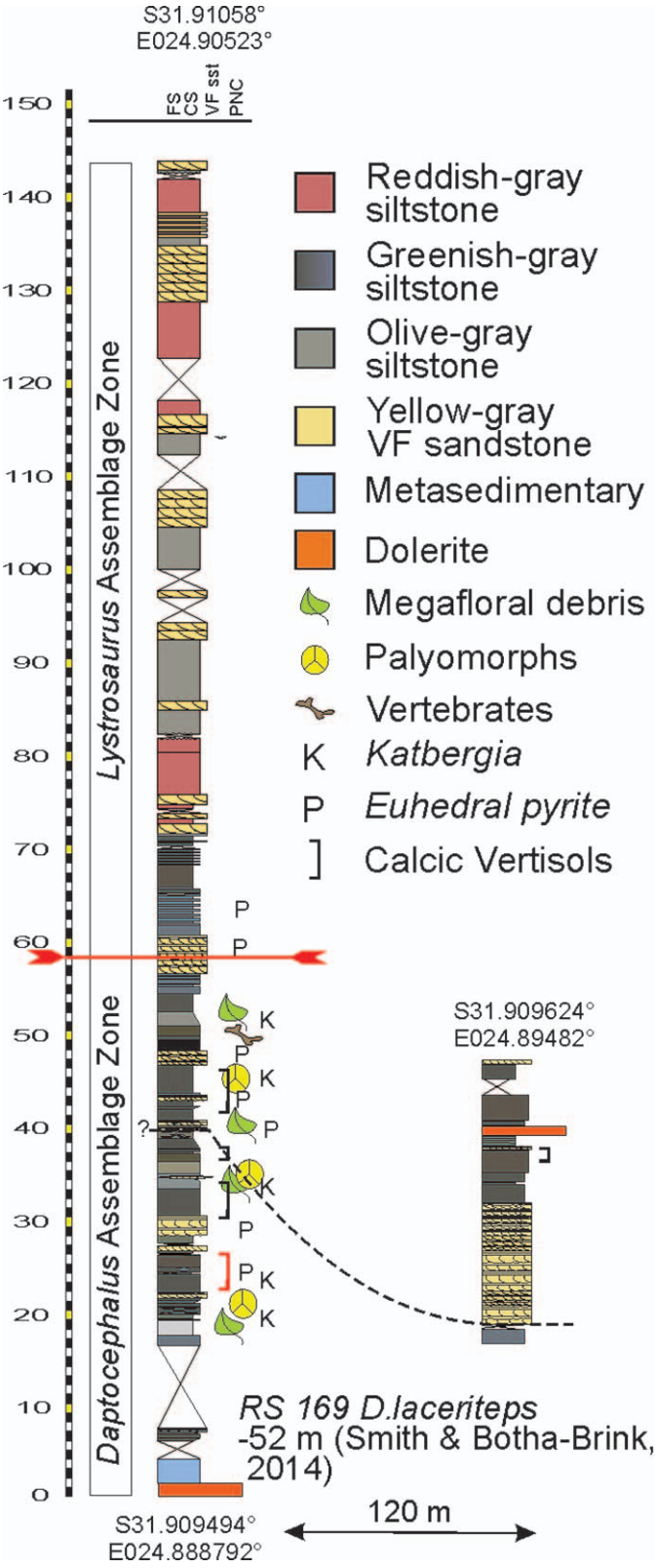

FIG. 3.—Measured stratigraphic section beginning on farm 527/Quaggasfontein (S31.90905, E024.88879, WGS 84) at an elevation of 1584 m, and it ends on farm Pienaarsbaken (S31.91058, E024.90523) at an elevation of 1718 m. Smith and Botha-Brink (2014) report specimen RS169 (*Dicynodon* (*Daptocephalus*; Viglietti et al. 2016) *laceriteps*), from the base of the section, as lying 52 m below the contact with the overlying *Lystrosaurus* Assemblage Zone, which they equate to the Permian–Triassic Boundary. The position of the boundary, as based on this record, is marked by a solid red line with double arrow tails. The calcic Vertisol interval occurs below the boundary and is eroded out to the southeast, in less than 120 m, by a 12-m-thick, multistoried very-fine grained fluvial channel. A short, laterally correlative measured section to the southeast shows this thick sandstone succession. Geochemical analyses reported, herein, originate from the basal paleosol interval marked as a red bracket. Scale in meters.

marble standard with $\delta^{18}O$ –2.07 ± 0.16 ‰ and $\delta^{13}C$ –2.52 ± 0.23 ‰, and reported with respect to the Pee Dee Belemnite standard (VPDB; Craig 1957); $\delta^{18}O$ is reported with respect to Vienna standard meteoric ocean water (SMOW; Gonfiantini 1984).

RESULTS

All pedogenically altered layers occur within the lowermost 45 m of the 527/Quaggasfontein stratigraphic section, spanning the farms Quaggasfontein and Pienaarsbaken (Fig. 3). The lowest pedogenically altered layer occurs ~ 20 m (19.2–20.8 m) above the base of the section, with seven other intervals of pedogenically altered intervals at higher positions: 23.4–24.5 m; 26.7–27.0 m (erosional upper contact); 29.6–33.9 m; 34.0–36.4 m; 36.6–38.6 m; 39.5–41.1 m; and 42.5–45.4 m (Figs. 3, 4). All pedogenically altered layers display similar field-scale lithological, morphological, and textural characteristics and patterns. Morphological features of these layers include pedogenic structure ranging from single-grain (massive) to wedge-shape aggregate structures with secondary medium-to-coarse angular blocky structures, arcuate slickenplanes with dip planes up to ~ 15° from horizontal and extending up to ~ 0.5 m in height and 2 m in length. These pedogenic layers include disorthic (*sensu* Brewer 1964) calcareous nodules and concretions (Fig. 4B–D) ranging in size from a few millimeters to a decimeter (Fig. 5). Carbonate nodules are common to abundant and show a coarse pattern of increasing size and abundance downward through each pedogenically altered layer. The colors of the pedogenically altered wackestone layers are generally greenish-gray (~ 5GY 4/1), with weak to moderate contrast dusky red (~ 10R 4/2); medium to coarse, irregularly-shaped mottles are common (~ 15% of exposed surface) toward the top and become increasingly rare downward through the profile. Considering these features in order of their most prominent to least prominent occurrence in terms of field-scale observations, these pedogenically altered layers qualify as gleyed calcic Vertisols in the paleosol-specific classification system of Mack et al. (1993; see also Tabor et al. 2017). A more detailed field and petrographic description is provided below to gain a deeper understanding of the morphological, textural, and geochemical characteristics.

The basal deposits of the gleyed calcic Vertisol that underlie and gradationally become the lowermost pedogenically altered horizons of the paleosol profile (Fig. 5) are dark greenish gray (5GY 4/1) to dusky yellow gray (5GY 3/2), sandy coarse siltstone in which millimeter-sized mud chips, millimeter-scale low angle cross lamination, and centimeter-scale bedding are seen in outcrop. Primary sedimentary structures are clear in thin section and include rippled surfaces, starved ripples, soft-sediment deformation, and millimeter-scale fining up lamination (Fig. 5G, H). Micro-XRF analysis of thin sections revealed the presence of a single, calcium-rich soil aggregate in one thin section (280517.4); soil aggregates (Gastaldo et al. 2013), though, are not common in thin sections (Fig. 6). This reflects the fact that many pedogenically altered layers are characterized by single-grain structure due to the coarse-grained lithologies from which they are composed. Ped structures are medium to large wedge-shaped and angular-blocky aggregates and, as such, are too coarse to be captured on the size of petrographic thin sections used in this study. Nevertheless, centimeter-scale diameter burrows are present both in

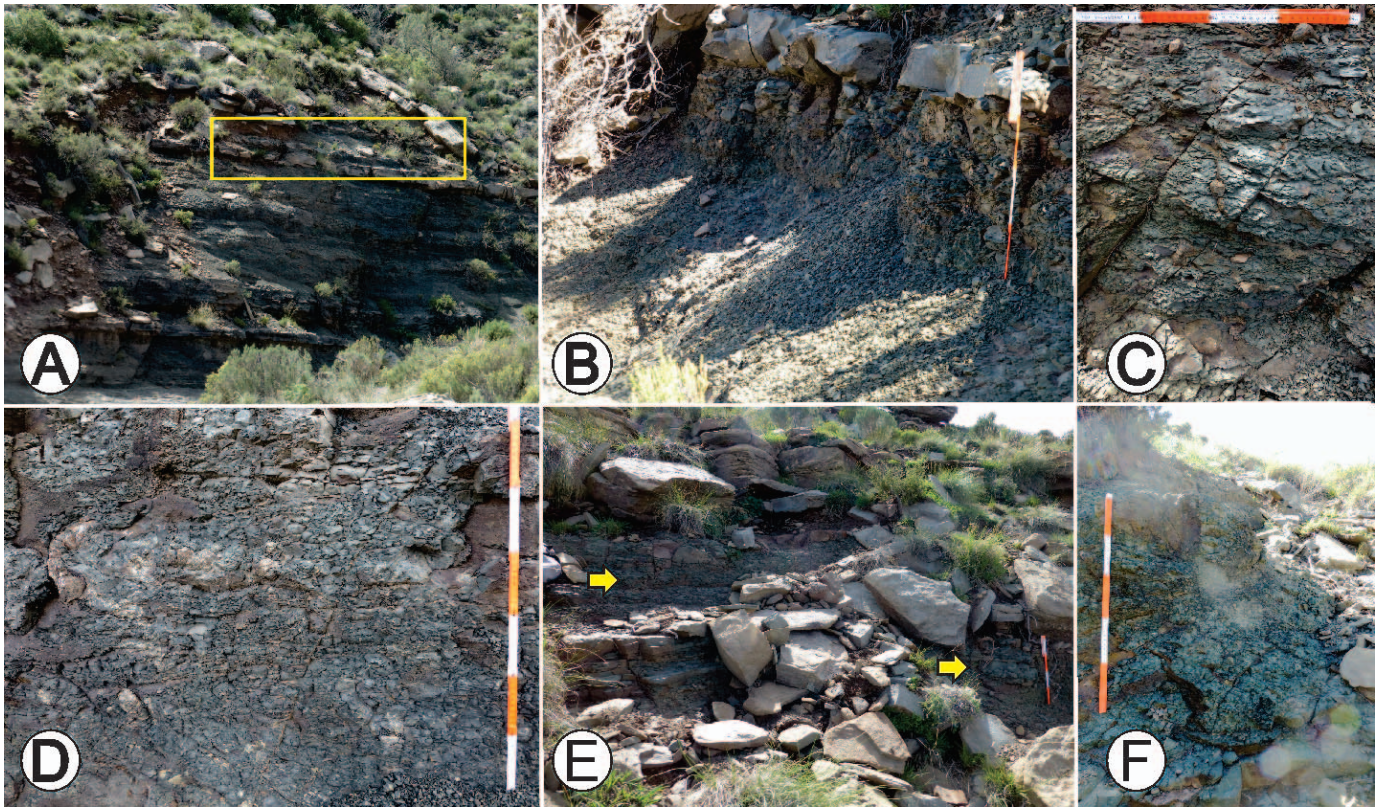

FIG. 4.—Field images of calcic Vertisol intervals. **A)** Calcic Vertisol interval exposed on northwestern face of erosional gulley, which is the focus of the current study. The paleosol lies above a thin sandstone bench, and can be traced laterally for ~ 35 m (S31.90886°, E024.89061°). **B)** Image of the upper 30 cm of calcic Vertisol exposure in Part A. **C)** Distribution of calcite-cemented nodules in greenish-gray, fissile siltstone at ~ 45 m stratigraphic height (S31.90885°, E024.893847°). **D)** Distribution of calcite-cemented nodules in greenish-gray, fissile siltstone at ~ 37 m stratigraphic height (S31.90894°, E024.89391°). **E)** Two calcic Vertisols, each overlain by an erosional wackestone, at ~ 45.4 m stratigraphic height (S31.90860°, E024.89120°). **F)** Limited exposure of calcic Vertisol at ~ 34.5 m stratigraphic height (S31.90868°, E024.89114°).

outcrop (Fig. 7A) and in thin section (Fig. 6C, E–G), with the cylindrical *Katbergia* (Gastaldo and Rolerson 2008) commonly encountered in both vertical and subhorizontal orientation. Carbonate cement is present in the burrow fill and in the surrounding siltstone matrix (e.g., Fig. 6G). In addition, unidentifiable millimeter-wide plant axes lie parallel to bedding, and pollen assemblages have been recovered from these deposits. The upper boundary of the paleosol with overlying lithologies is clear and wavy, whereas the overlying material is homogeneous and monotonous lithologically, with little color variation. Large (10–20 cm diameter) spherical calcareous nodules are concentrated near the contact with the underlying paleosol profile.

The lowermost paleosol profile in the 527/Quaggasfontein section is variably thick, 100–120 cm, due to a wavy erosional upper contact back-filled by a lenticular siltstone (Fig. 5). In general, the materials in the paleosol profile are coarse to fine, dark greenish-gray siltstone to wackestone which, in some cases, may exhibit discrete reddish-gray (10R 4/2) vermicular mottled horizons up to several decimeters thick. Homogeneous (Fig. 6D) and bioturbated (Fig. 6A–C, F) fine siltstone is predominant in the succession, with point counts of silt in thin section dominated by quartz grains with varying opaque and feldspar + mica components (Fig. 8). A down-profile trend of increasing proportions of opaques and weathering products occurs in the Bkss and Btk horizons (Fig. 5). Also present are occasional degraded plant remains, isolated 0.5-mm-scale pyrite (Fig. 6E), 2-mm-diameter mud chips, and fractured peds. In thin section, burrows may be up to 3 mm in diameter and are filled with coarse silt. Slickensides are present (Fig. 7C), scattered calcite-cemented nodules are ubiquitous, and bedded nodular horizons characterize the paleosol at several horizons. Three sizes of discrete nodules occur, the surfaces of which may appear light olive gray (5Y 6/1), yellowish-gray (5Y 8/4), or bluish-white (5B 9/1) upon exposure and weathering. Centimeter-diameter nodules, generally, are scattered throughout, whereas nodules ranging from 5 to 20 cm in diameter are concentrated at, although not restricted to, the lower parts of the paleosol (Fig. 7B). The larger-diameter nodules are dark greenish gray (5GY 4/1) to medium gray (N5) and micritic, and may show signs of central cracking and spar-fill (Fig. 7D). Millimeter-diameter unidentifiable and centimeter-diameter sphenopsid-plant axes occur in the upper parts of paleosols where the density of nodules decreases, and millimeter-diameter vertical and subhorizontal rooting may be preserved sporadically. Due to the fissile and highly fragmentary nature of the matrix, rooting characteristics cannot be detailed.

Geochemical Trends

The geochemical trends of one well-defined calcic Vertisol interval, occurring between 24.35 and 25.2 m (Figs. 4A–C, 7, 8), are presented. Unlike the Protosols reported by Gastaldo et al. (2014) at New Wapadsberg Pass, 1.9 km to the east where O horizons are preserved that allow for the recognition of stacked-soil boundaries, neither an O nor an A horizon are recognized at Quaggasfontein. Rather, the paleosol base is identified by the presence of primary sedimentary structures, interpreted as the C horizon (Figs. 5, 6G, H), and the upper soil horizons by siltstone samples in which primary structures are not preserved. A down-profile trend in weathering products with an increasing proportion of opaques is used to circumscribe

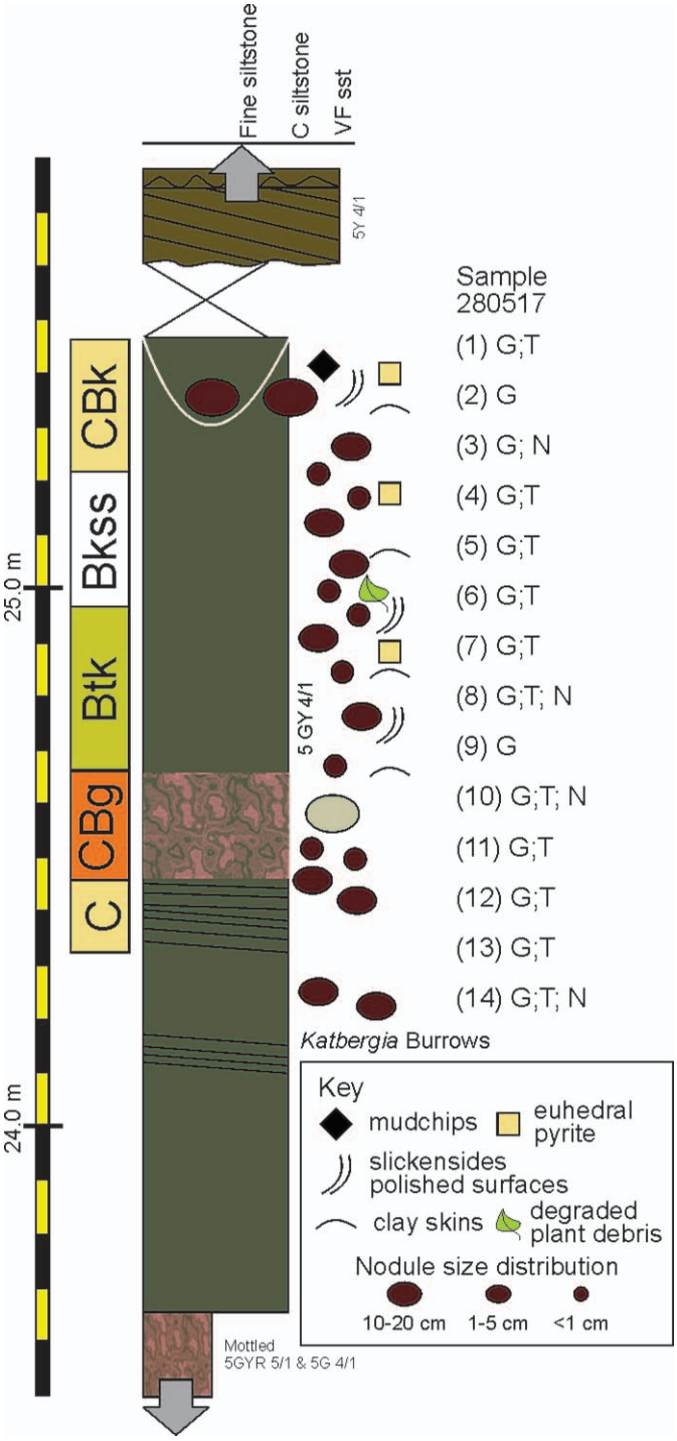

FIG. 5.—Centimeter-scale measured section of the basal paleosol interval in which the most complete profile occurs. A thin, lenticular siltstone eroded into the top of the profile, and is indicated by a white arc. Fourteen samples are identified from which whole-rock geochemistry (G) and thin sections (T) were completed, and representative nodules (N) were cut, surfaces polished, and $\delta^{13}C$ and $\delta^{18}O$ stable-isotope analyses undertaken. Sample numbers coordinate with thin sections imaged in Figure 6. Scale in decimeters.

the Vertisol interval (Fig. 8, curved arrow). Hence, the calcic Vertisol detailed herein, has a total thickness of 80 cm (Figs. 9, 10; Table 1).

Carbon.—All weight %TOC values are < 1%, with an overall trend of decreasing values down the paleosol profile. A maximum value of 0.87% is attained at a depth of 20 cm below the top of the soil, reflecting organic-carbon concentration in the B horizon (Fig. 9A). The values for weight %LOI follow the same trend, with maximum values (6.28 % carbon and water, possibly sulfate or SO_2 from pyrite noted in petrography) in the upper 30 cm, and minimum values (3.07 %) in the lower parts of the profile (Table 1).

Molecular Weathering Ratios.—Plots of base loss (Fig. 9) are a proxy for the leaching of major base elements—including Mg, Na, K, and Ca—relative to Ti, and two distinct trends can be seen in the profile for bulk non-calcareous paleosol matrix. There is a distinctive trend in decreasing translocation of Ca relative to Ti, which appears to be in two steps (Fig. 9B). The upper 30 cm of the interval shows markedly higher, whereas the lower 50 cm show markedly lower, proportions of Ca/Ti values; Na, Mg, or K relative to Ti do not show a trend similar to that of Ca/Ti. Rather, Na remains relatively constant to a depth of 50 cm and, thereafter, increases towards the bottom of the paleosol profile; both Mg and K remain relatively constant showing a slight decrease in values downward through the profile. Base loss uses only bulk-rock compositional data and excludes any material associated with paleosol nodules. Hence, the Ca/Ti trend reflects only that of the matrix, which also plots similarly to profile trends for calcification (Fig. 9E). Other molecular weathering ratio trends show a two-stepped change over the profile, although the position at which these excursions occur is not always coincident.

Trends in clayeyness (Al/Si) and mineral maturity (Si/Al) mirror each other in the profile (Fig. 9C, G). There is a decrease in mineral maturity to a minimum value at 50 cm below the top of the soil, whereafter the values increase. In contrast, an increasing trend in clayeyness occurs to a depth of 50 cm, whereafter values decline. Values for salinization ([K+Na]/Al) do not vary significantly in the uppermost 50 cm and increase towards the base of the profile (Fig. 9F). Similarly, mineral-assemblage stability (Fe/K) values show a decreasing trend in the upper 20 cm, beneath which the maximum value occurs (Fig. 9D). Thereafter, mineral-assemblage stability values decrease to a depth of 60 cm and, then, increase up to near the maximum value in the profile. CIA-K values calculated for this Vertisol profile range from a low value of 64 at a depth of 10 cm to a high value of 82 at a depth of 50 cm, which is the same horizon at which there is an inflection point in the molecular weathering ratios and highest mineral-stability values. CALMAG values range from a low of 51 at a depth of 20 m to a high value of 68 at a depth of 80 cm (see Fig. 9E).

Mass-Balance Trends.—Mass-balance plots show the relative translocation of major cations down the paleosol profile relative to Ti, which is considered to be an immobile element (Driese et al. 2005). Mass-balance values are calculated using geochemical data from the C horizon, interpreted in the profile where primary structures are preserved (Figs. 5, 6). Due to the high variability in relative cation enrichment or depletion depending on which immobile element is used in the calculation, only the major trends are described here. Studies of modern Vertisols often have chosen to use Ti (Driese et al. 2000). This is because calculations using Zr are demonstrated to be biased when sand and coarse-silt clasts are present (Stiles et al. 2003a) and the distribution of zircon minerals amongst the profile lithologies is often heterogeneous. In contrast, Ti generally is preserved in the clay-rich intervals and is better suited for mass-balance calculations of volume change and mobile-element translocation during petrogenesis (Stiles et al. 2003a, 2003b). Hence, although plots for both

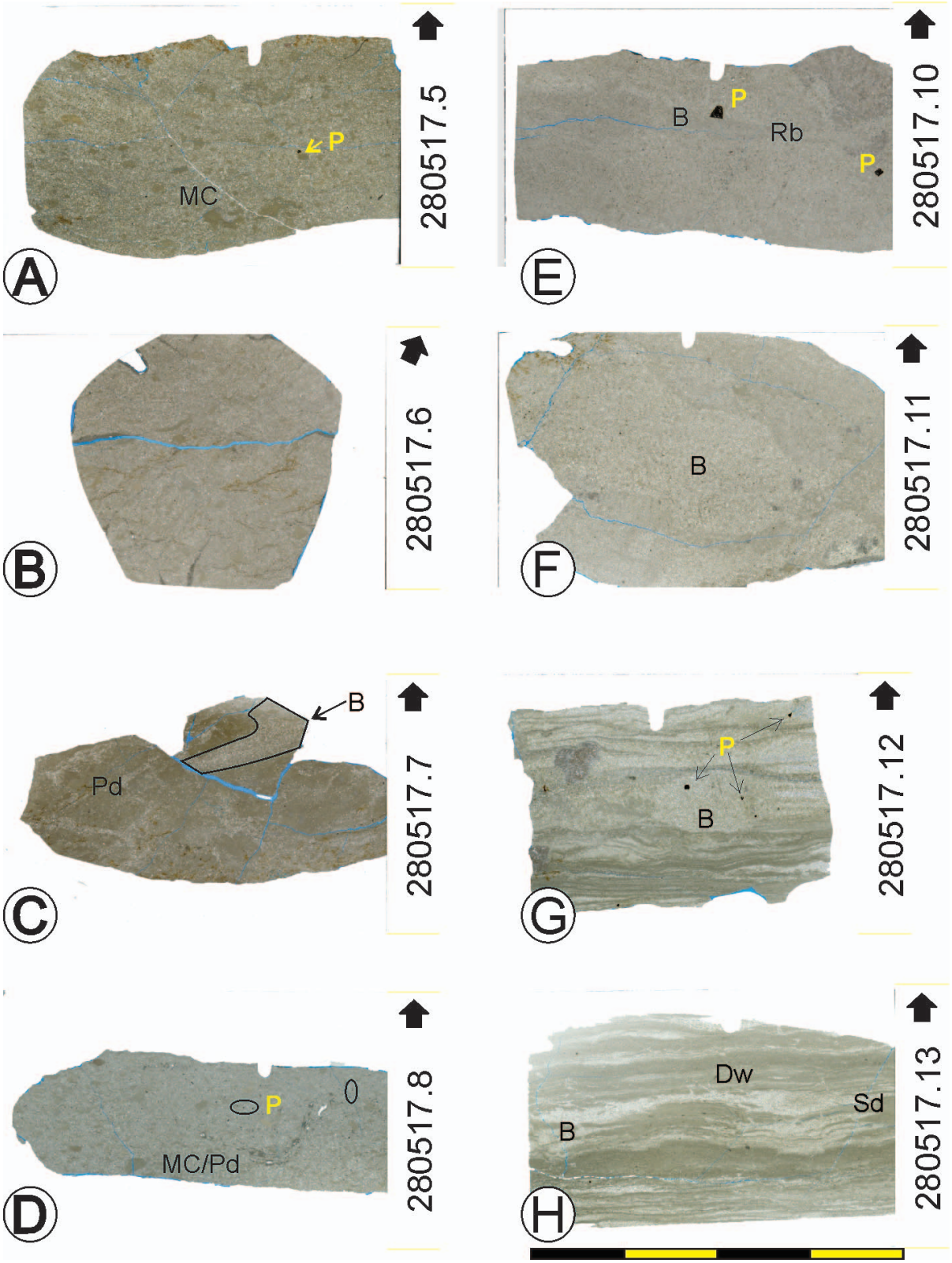

FIG. 6.—Representative thin sections of each Vertisol horizon identified in Figure 4. **A)** Sample 280517.5 in the Bkss horizon shows homogenization, millimeter-scale mudclasts (MC), and opaque sub-millimeter scale euhedral pyrite (P). **B)** Sample 280517.6 near the contact between the Bkss and underlying Btk horizons in which clay linings and homogenization occur. **C)** Sample 280517.7, showing peds (Pd) and inclined silt-filled burrows (B). **D)** Sample 280517.8 from the lower part of the Btk horizon where mudclasts or peds (MC/Pd) occur in a silty matrix with opaque sub-millimeter scale, opaque euhedral pyrite crystals (P). **E)** Sample 280517.10 from the mottled Bw horizon in which relict bedding (Rb) is crosscut by a millimeter-scale vertical burrow (B) and sub-millimeter scale opaque, pyrite crystals occur. **F)** Sample 280517.11 from the mottled Bw horizon in which a centimeter-scale, inclined silt-filled burrow is observed. **G)** Sample 28057.12 from the underlying C horizon in which basal lamination is overlain by centimeter-scale ripples. A centimeter-scale burrow (B) that is silt-filled contains sub-millimeter scale, opaque pyrite (P). **H)** Sample 290517 from the base of the C horizon in which sub-millimeter scale lamination and ripples are preserved, along with either soft-sediment (Sd) or dewatering (Dw) structures. Vertical, sub-millimeter scale burrows (B) cross cut lamination. Scale in cm; arrows on slide indicate stratigraphic up.

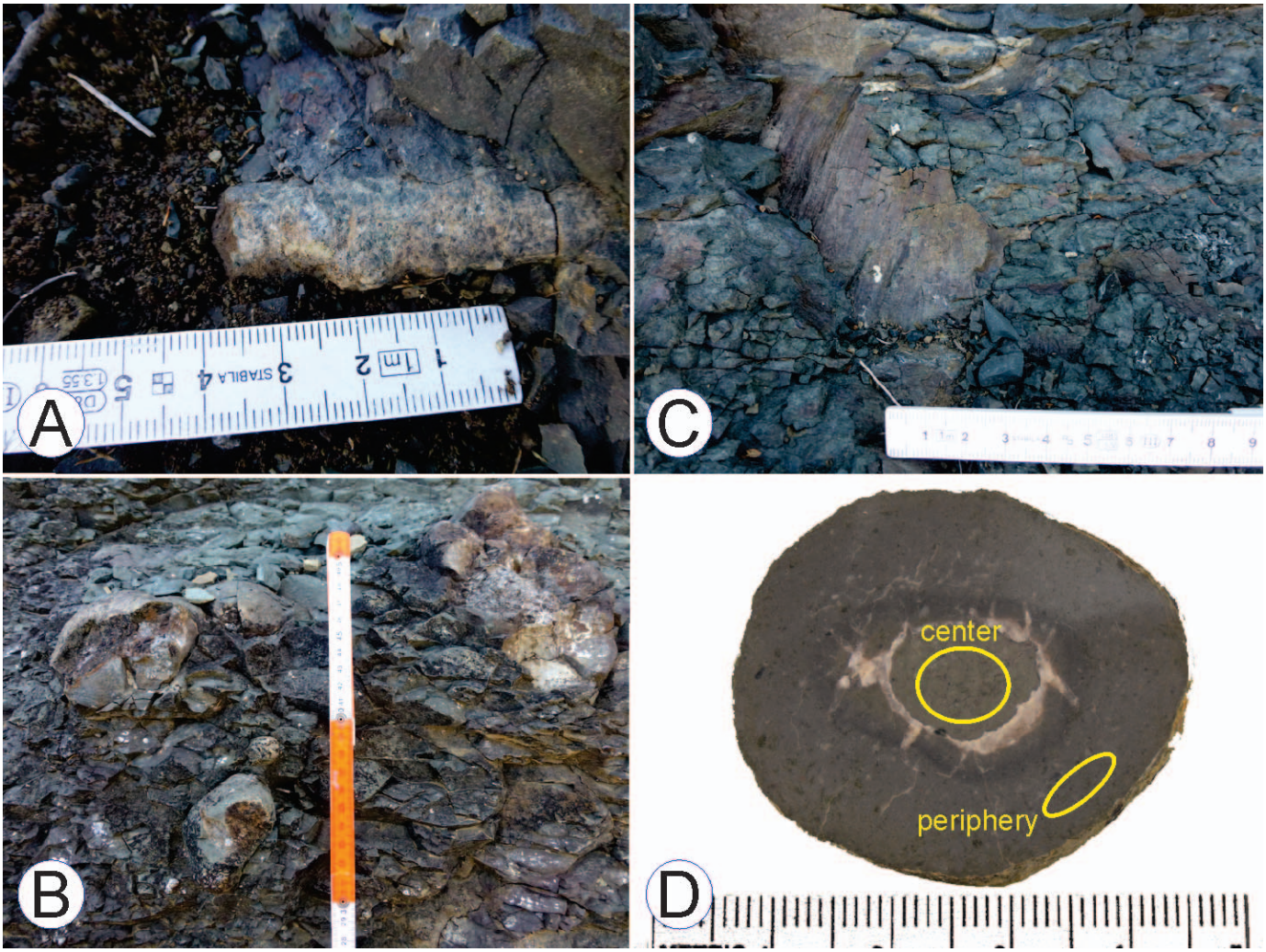

FIG. 7.—Macroscopic features of upper *Daptocephalus* Assemblage Zone calcic Vertisols. **A)** *Katbergia* burrows of > 1 cm diameter in the basal intervals. **B)** Scattered small (1–2 cm diameter) and large (5–20 cm diameter) calcite-cemented nodules in the Btk horizon. Large-diameter nodules in the upper part of the image define a horizon that can be traced laterally across the limited outcrop. **C)** Slickensides of a grayish-red color crosscutting greenish-gray siltstone. **D)** Cut and polished surface of a septarian cracked nodule, with a light greenish-gray surface color, from the Bw horizon from which stable $\delta^{13}C$ and $\delta^{18}O$ stable-isotope analyses were done (Table 1). Scales in millimeters, centimeters, and white-and-orange decimeters.

sets of calculations were undertaken (Fig. 9A–H), the results focus on the trends exhibited in the graphs using Ti as the immobile element (Fig. 10).

Four proxies are presented from these mass-balance calculations: redoximorphy, clay accumulation, carbonate leaching, and biocycling. Redoximorphy measures the translocation of Mn and Fe (Fig. 10A), and although Fe relative to Ti appears to be somewhat enriched near the top of the soil profile, Mn exhibits a marked two-step plot similar to those data on molecular weathering ratio (e.g., Fig. 9E, H). Here, an increase in Mn is found in the upper 30 cm of the soil profile, whereafter there is a significant decrease in the element to a relatively constant value approaching zero. That negative excursion in Mn begins beneath a nodular horizon in which concretions attain a length of 20 cm. Clay accumulation measures the translocation of Si, Al, Na, and K (movement of authigenically formed and detrital phyllosilicates downward through the soil). Once again, there is a two-stepped trend in all of these values with significant changes below a depth of 50 cm (80 cm in graphs; Fig. 10B) in the soil profile. Si exhibits a relatively constant value across the interval, with the maximum value at 60 cm depth in the profile (90 cm in graph). Both Al and K are enriched in the upper 50 cm of the profile and decrease towards the bottom of the paleosol, indicating a decrease in phyllosilicate in the lower part of the profile. In contrast, Na exhibits a trend opposite to those of Al and K, with negative values in the upper soil horizons and a distinct positive excursion at a depth of 60 cm (90 cm in graphs; Fig. 10B). Carbonate leaching measures the translocation of Ca and Mg. Mg is slightly enriched from 10 to 50 cm beneath the paleosol top (40–80 cm in graphs) and decreases to values near zero below in the profile. Ca in the matrix, however, is relatively concentrated between 10 and 30 cm from the profile top and decreases to the lower soil horizons (Fig. 10C). Biocycling tracks the translocation of P and, again, there is a two-stepped trend in these data (Fig. 10D). The uppermost 30 cm of the interval shows an oscillation in positive values of P relative to Ti, followed by a distinct negative excursion at –30 cm. A decrease from positive to negative values occurs in the underlying siltstone (–40 to –100 cm).

Stable-Isotope Geochemistry.—Four large calcite-cemented nodules were analyzed. Two nodules originate from the calcic Vertisol, collected at a depth of 40 cm in the profile, and two of which were collected in a nodular horizon in an incomplete soil profile immediately above the top of

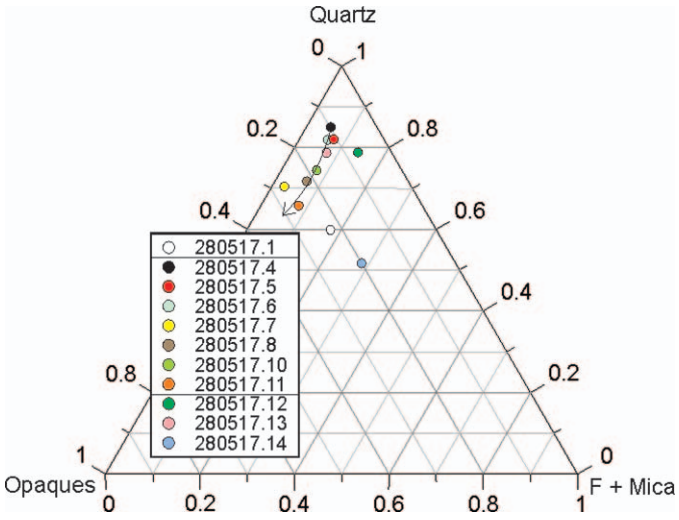

FIG. 8.—Ternary diagram plotting quartz, opaques, and feldspar+mica of thin-section point counts (N = 3134) of coarse-silt-sized grains along paleosol profile. Arrow indicates a down-profile trend in the relationship of these clasts, and the boxed samples in the legend delimit the upper and lower boundaries of the calcic Vertisol profile detailed herein.

the interval. Only micrite cements were sampled, and both the centers and periphery of the nodules were analyzed (Fig. 7D). Values for $\delta^{13}C$ (‰VPDB) range from –8.6 to –5.4, and values for $\delta^{18}O$ (‰VPDB) range from –21.2 to –21.7 (Table 2).

DISCUSSION

The recognition of a succession of calcic Vertisols in the Upper *Daptocephalus* Assemblage Zone, along with the petrographic and geochemical characterization of one paleosol interval, allow for an assessment of their stratigraphic and paleoclimatologic implications for the Changhsingian of the Karoo Basin. When we compare our results with previous climate interpretations for this time, estimates of mean annual temperature (MAT) and mean annual precipitation (MAP) differ from those previously proposed by other workers using different proxy data (see below). Herein, we propose a landscape-drainage model for the latest Permian landscape to account for the variance in observed physical and geochemical features of these polygenetic soils.

Stratigraphic Implications

Late Permian (Lower Beaufort) and Early Triassic paleosols in the Karoo Basin were reported first by Smith (1990, 1995), who recognized three Permian and one Triassic pedotype. Originally, each pedotype was interpreted to represent a component of a lateral gradient across one floodplain landscape in the *Pristerognathus* Assemblage Zone, Lower Beaufort Teekloof Formation (Wuchiapingian; Rubidge et al. 2013). Smith (1990) envisioned a relatively immature greenish calcic paleosol (= Protosol; after Mack et al. 1993; Tabor et al. 2017) in which vertical calcareous tubules, rhizoconcretions, and small (< 10 cm diameter) calcareous nodules characterized pedogenesis along a channel bank or levee. Proximal to this soil type, and interpreted as having formed adjacent to meanderbelt slopes, were paleosols of a reddish-brown (maroon) color in which slickensides and calcareous glaebules are common (= Vertisol). In the more distal parts of the floodbasin, dark brown to green paleosols are reported in which laminated green siltstone and sandstone beds and calcareous nodules are less common, and are often accompanied by small septarian nodules and "rosettes" of quartz pseudomorphs after gypsum (= Gypsisols; Smith 1990). Subsequently, this paleosol continuum also was interpreted to occur in the upper Beaufort Formation of the *Dicynodon* (*Daptocephalus*) Assemblage Zone (Smith 1995). A single pedotype replaced these in the overlying *Lystrosaurus* Assemblage Zone, interpreted by many workers as Triassic in age (but see Gastaldo et al. 2015, 2017, 2018, 2019b, 2020). That pedotype is characterized as mainly reddish-gray and exhibiting sporadic green mottling around rhizoconcretions, in which horizons of well-developed calcite nodules and sand-filled desiccation cracks occur (= Calcisol; Smith 1995). Subsequently, Retallack et al. (2003) proposed an array of latest Permian and earliest Triassic pedotypes for the stratigraphic interval encompassing the transition from the *Daptocephalus* to *Lystrosaurus* Assemblage Zones. We retain the classification of Mack et al. (1993) and Tabor et al. (2017) because the paleosol scheme of Retallack et al. (2003) has been shown to be non-utilitarian and ambiguous (see discussion in Gastaldo et al. 2014). As such, it has not been applied to paleosols in the basin by subsequent workers (e.g., Ward et al. 2005; Smith and Botha 2005; Smith and Botha-Brink 2014; Viglietti et al. 2016, 2018).

The gleyed calcic Vertisols in the 527/Quaggasfontein section share physical characteristics with previously described pedotypes in the Teekloof Formation (Smith 1990). The presence of abundant and scattered 1–5-cm-diameter spherical nodules, rare horizons of bedded larger nodules, occasional septarian concretions, and slickensides compare well with features described for that formation's proximal floodbasin facies (Smith 1990; = Entisols of Smith 1995). Mottling is a reported feature of the distal-floodplain pedotype (Smith 1990), although this character is a function of redox conditions in response to water-table oscillation rather than to any specific position along a floodplain gradient (e.g., Tabor et al. 2017; Gastaldo et al. 2019a). Hence, these upper *Daptocephalus* Assemblage Zone paleosols, as defined by their stratigraphic position relative to the boundary between vertebrate-assemblage zones (Viglietti et al. 2016, 2018), exhibit the general characteristics of many Late Permian paleosols. As discussed below, several additional macroscopic features are components of these intervals.

The ichnotaxon *Katbergia*, interpreted by Gastaldo and Rolerson (2008) as a decapod crustacean burrow inhabiting wet (oxygenated) soil conditions, is common. Its centimeter-diameter burrow casts (Figs. 6F, 7A) are preserved in the limited exposures of four of the seven gleyed calcic paleosols. These trace fossils, generally, are restricted to the lower half of each interval. In contrast, adpressions of millimeter- to centimeter-diameter plant axes are encountered where *Katbergia* burrows were not observed, indicating that these paleosols experienced a range of pore-water geochemistries from oxic to dysoxic or anoxic (Gastaldo and Rolerson 2008). Fluxes in redox conditions also are indicated by the presence of small, 0.5 mm crystals of euhedral pyrite (a petrographically opaque mineral) in both burrow fills and surrounding matrix (Fig. 6E, G) where there was activity of sulfur-reducing bacteria. Pyrite crystals often are found at bedding contacts and scattered across their surfaces in crossbed sets of the very-fine-sandstone bodies of the 527/Quaggasfontein–Piernaarbaken, and other, stratigraphic sections in the area (Kus et al. 2017). These pyrite concentrations in bedload deposits indicate a paleoenvironmental origin associated with landscape degradation, erosion of calcic Vertisols in response to changes in fluvial gradient (Gastaldo and Demko 2011), and depositional stasis in fluvial channel systems. To date, isolated or distributed pyrite, either in paleosol profiles or fluvial deposits, has not been reported from the *Daptocephalus* Assemblage Zone, and its genesis is still not understood fully.

The unexpected occurrence of pyrite throughout the lowermost 70 m of the stratigraphy at 527/Quaggasfotnein indicates that there must have been: 1) a significant and somewhat repetitive or persistent sulfur source, 2) early diagenetic conditions promoting sulfur-reducing bacterial activity, and 3) periodic pore-water anoxia. Thomas et al. (2011) note that sulfur in modern soils typically originates from a marine source. However, there is no

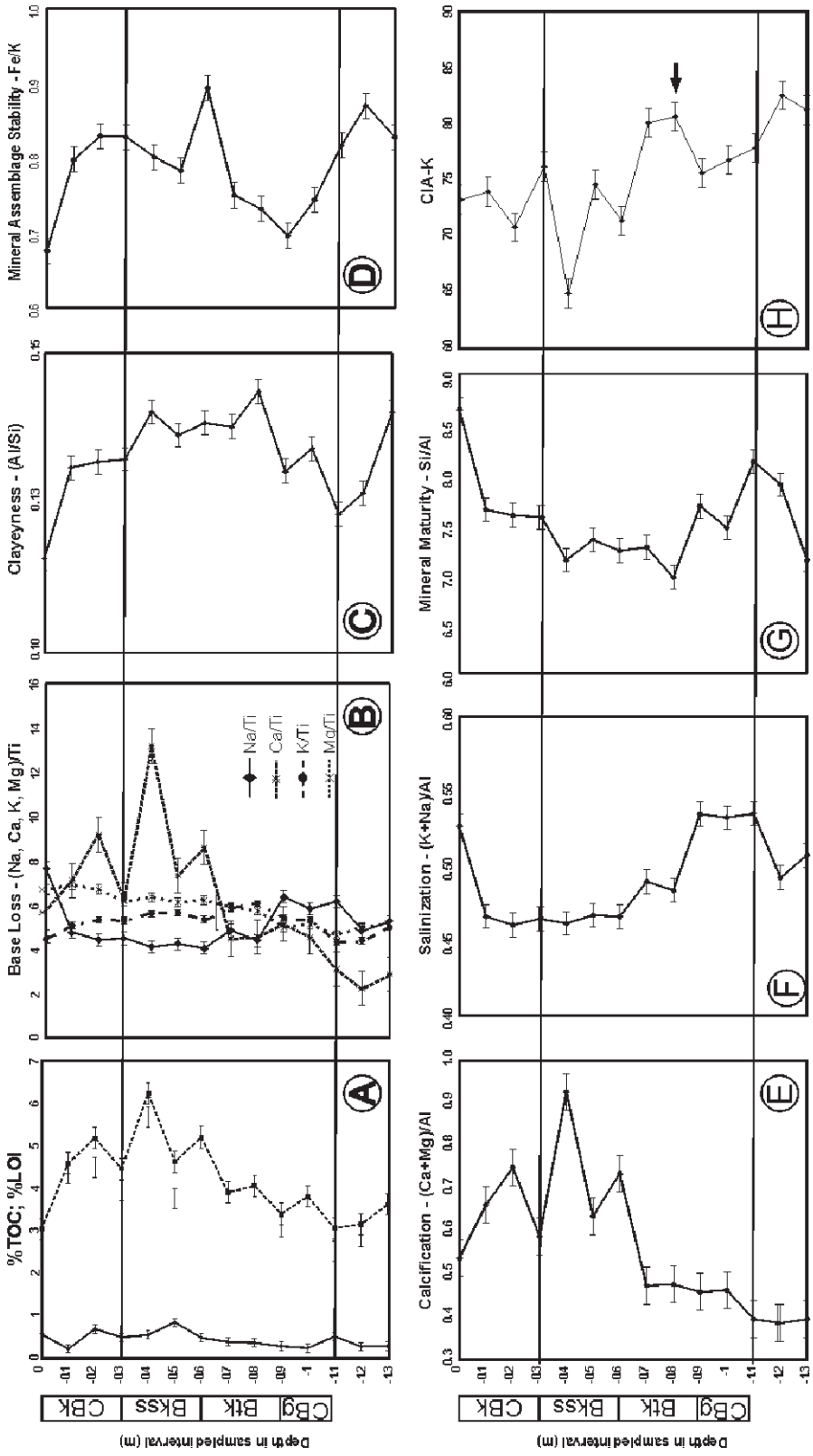

FIG. 9.—Geochemical proxy profiles of Quagasfontein gleyed calcic Vertisol shown in Figure 5 (see text for details). The top and base of the paleosol described in the text is marked by solid lines across the plots. **A)** Percent total organic carbon (TOC; solid line) and percent carbon on a loss-on-ignition (LOI; dashed line) basis at 10-centimeter sampling intervals, with standard error bars. **B)** Base-loss profiles for Na/Ti (solid black line), Ca/Ti (short dash line), K/Ti (long dash line), and Mg/Ti (dotted line), with standard error bars. **C)** Clayeyness (Al/Si). **D)** Mineral-assemblage stability (Fe/K). **E)** Calcification ([Ca + Mg]/Al). **F)** Salinization ([K + Na]/Al). **G)** Mineral maturity (Si/Al). **H)** Chemical Index of Alteration minus Potassium (CIA-K). Data are provided in supplemental data Tables.

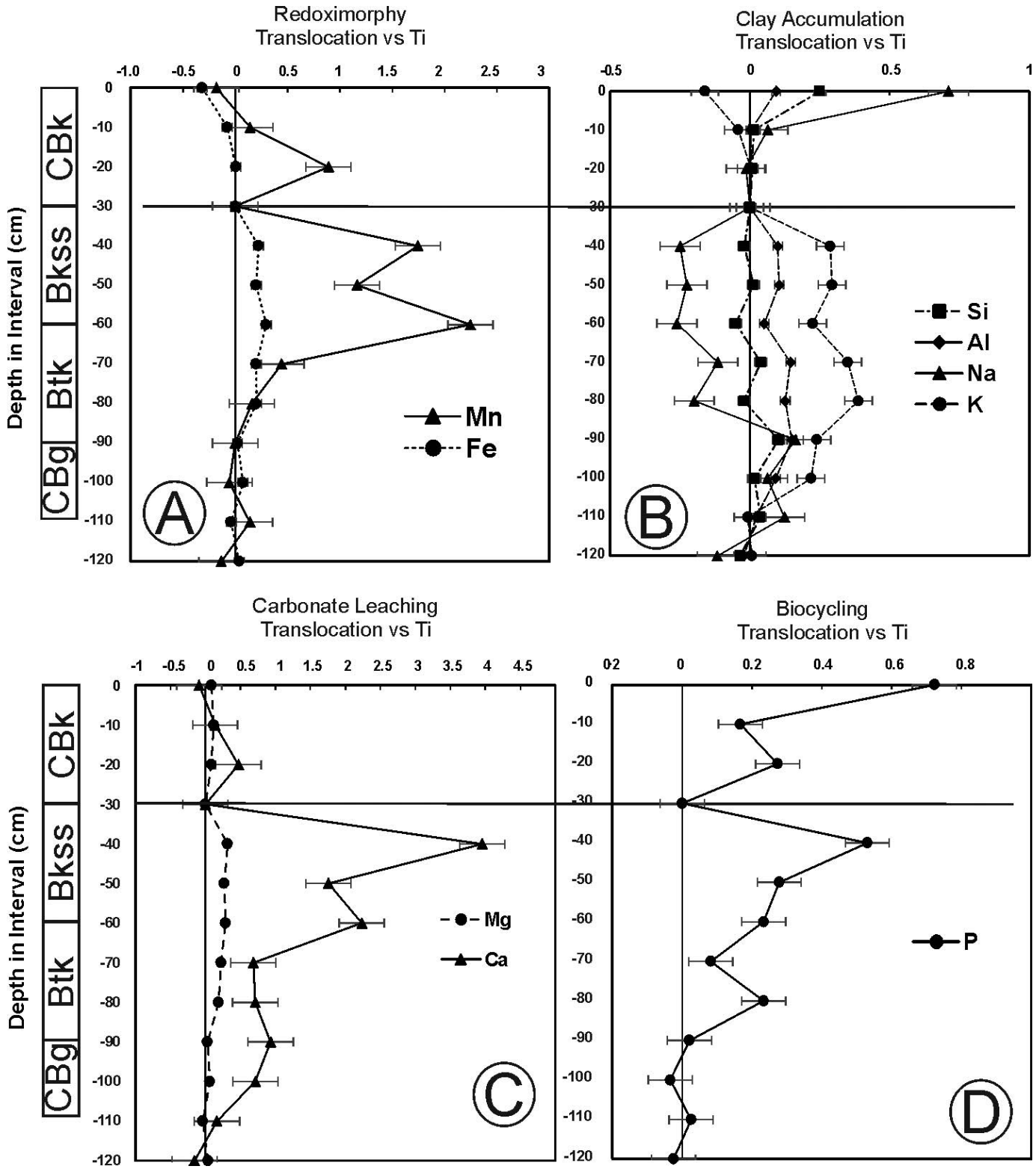

FIG. 10.—Mass-balance plots for redoximorphy, clay accumulation, carbonate leaching, and biocycling versus profile depth following Driese et al. (2000). Data were calculated against C horizons identified at depths of 30 cm and 110–120 cm. **A)** Translocation of Mn and Fe through the calcic Vertisol profile versus Ti as the immobile element. **B)** Translocation of Si (dashed line), Al (long dashed line), Na (solid line), and K (short dashed line) across the Vertisol profile using Ti as the immobile element. **C)** Translocation of Mg and Ca in the 1.3-m calcic Vertisol profile using Ti as the immobile element. **D)** Translocation of P in the calcic Vertisol profile using Ti as the immobile element.

TABLE 1.—*Results of major-element-oxide (including Ti and Zr) ICP-MS analyses, ALS Laboratories, Las Vegas, Nevada (January 27, 2018) and total organic carbon (TOC) and total organic nitrogen (TON), Perkin Elmer 2400 Elemental Analyzer, Colby College.*

	ME-ICP06	ME-ICP06	ME-ICP06	ME-ICP06	ME-ICP06	ME-ICP06	ME-ICP06	ME-ICP06	ME-ICP06	ME-ICP06	ME-ICP06	ME-ICP06	ME-ICP06	OA-GRA05	TOT-ICP06	PerkinElmer 2400		ME-MS81
SAMPLE	SiO2	Al2O3	Fe2O3	CaO	MgO	Na2O	K2O	Cr2O3	TiO2	MnO	P2O5	SrO	BaO	LOI	Total	TOC	TON	Zr
DESCRIPTION	%	%	%	%	%	%	%	%	%	%	%	%	%	%	%	%	%	ppm
280517.1	70.3	13.8	2.82	1.87	1.59	2.8	2.46	< 0.01	0.47	0.05	0.18	0.05	0.06	3.07	99.52	0.59	0.04	252
280517.2	65.5	14.55	4.37	2.69	1.88	2	3.23	0.01	0.54	0.08	0.14	0.03	0.06	4.62	99.7	0.24	0.05	213
280517.3	63.9	14.3	4.67	3.41	1.79	1.82	3.32	0.01	0.53	0.13	0.15	0.03	0.06	5.22	99.34	0.71	0.06	192
280517.4	64.6	14.5	4.73	2.36	1.68	1.88	3.37	0.01	0.54	0.07	0.12	0.03	0.06	4.49	98.44	0.51	0.06	193
280517.5	59.9	14.25	4.77	4.9	1.7	1.69	3.51	0.01	0.53	0.11	0.15	0.04	0.16	6.28	98	0.57	0.07	189
280517.6	64.2	14.85	4.86	2.83	1.7	1.81	3.66	< 0.01	0.55	0.09	0.13	0.03	0.07	4.66	99.44	0.87	0.09	214
280517.7	62.4	14.65	5.44	3.44	1.79	1.79	3.59	0.01	0.57	0.14	0.13	0.02	0.06	5.24	99.27	0.5	0.05	170
280517.8	65.9	15.4	4.86	1.73	1.64	2.07	3.82	0.01	0.55	0.06	0.11	0.03	0.07	3.93	100.18	0.4	0.08	213
280517.9	64.4	15.7	5.05	1.82	1.65	1.94	4.07	0.01	0.57	0.05	0.13	0.02	0.08	4.09	99.58	0.38	0.05	195
280517.1	67.4	14.9	3.99	1.91	1.33	2.62	3.38	0.01	0.53	0.04	0.1	0.04	0.07	3.43	99.75	0.3	0.05	269
280517.11	65.7	14.95	4.43	1.79	1.45	2.53	3.51	0.01	0.56	0.04	0.1	0.04	0.07	3.84	99.02	0.26	0.07	258
280517.12	69.4	14.5	4.1	1.26	1.36	2.77	2.96	< 0.01	0.58	0.05	0.11	0.04	0.06	3.09	100.28	0.53	0.04	228
280517.13	67.9	14.6	4.66	0.96	1.54	2.29	3.16	0.01	0.61	0.04	0.11	0.03	0.06	3.18	99.15	0.3	0.05	190
280517.14	66	15.7	5.04	1.23	1.57	2.48	3.59	0.01	0.61	0.04	0.12	0.04	0.07	3.65	100.15	0.3	0.08	232

evidence for any marine influence in this part of the Karoo Supergroup; marine-influenced waters are responsible for deposition of the older Dwyka and Ecca groups in the Karoo Basin (Fig. 1). The Beaufort and overlying lithostratigraphic groups are fully continental in origin. Where a marine source is absent, an alternative sulfur source is atmospheric dust or sulfur-rich aerosols (Thomas et al. 2011). Maruoka et al. (2003) report elevated sulfur concentration in rocks at, and just below, the vertebrate-defined PTB in two sections at the town of Senekal in the northern Free State Province where outcrops represent a more condensed stratigraphy. In contrast, Coney et al. (2007) were not able to replicate these results from the more complete stratigraphic record exposed at Old Wapadsberg Pass. Enhanced sulfide values were attributed by Maruoka et al. (2003) to acid rain as a consequence of volcanism and, specifically, the emplacement of the Siberian Traps. Another, perhaps more likely, sulfur source for the Old Wapadsberg Pass succession is repeated Late Permian volcanic activity in the Cape Fold Belt where a final phase of orogenesis is dated at ~ 253 Ma (Blewett and Phillips 2016).

Paleoclimate Implications

Paleosol geochemical data can be used to estimate several paleoclimate components, or factors, including mean annual precipitation (MAP) and mean annual temperature (MAT; Sheldon and Tabor 2009), using molar ratios of CIA-K and salinization, respectively. MAP estimates are derived from CIA-K and CALMAG values, and are calibrated for precipitation values between 200 and 1600 mm/year using the equation

$$\mathrm{MAP(mm/year)} = 221^{e0.0197}(\mathrm{CIA\text{-}K}) \quad (6)$$

where the CIA-K = 100 x $[Al_2O_3/(Al_2O_3 + CaO + Na_2O)]$ with an error of ± 181 mm/year (Sheldon and Tabor 2009). Nordt and Driese (2010) also developed an empirical equation relating MAP to CALMAG:

$$\mathrm{MAP} = 22.69 * \mathrm{CALMAG} - 435.8 \quad (7)$$

with a standard error of ± 108 mm/yr and an $R^2 = 0.90$ for the empirical fit. The CIA-K and CALMAG values of the Bt horizon are used to calculate MAP (Sheldon and Tabor 2009), which is 50 cm below the top of the Quaggasfontein soil profile (Fig. 9 at arrow; Table 3). The MAP estimate from the Vertisol soil profile is 1080 ± 181 mm/year using CIA-K and is similar (1110 ± 108 mm/year) to the CALMAG value at the same position in the paleosol profile.

MAT is estimated from salinization values, S (Fig. 9F) as follows:

$$\mathrm{T(°C)} = -18.5\ \mathrm{S} + 17.3 \quad (8)$$

where S is the salinization ([K+Na]/Al) value of the Bt horizon (located 30–60 cm from the paleosol top) and standard error is ± 4.4° C with an $R^2 = 0.37$ for the empirical fit (Sheldon and Tabor 2009). Similar to above, the salinization value originates from the same position in the Bt horizon, 50 cm below the top of the soil profile (Fig. 9 at arrow; Table 3). The estimate of MAT is 10 ± 4° C.

Values of $\delta^{13}C$ obtained from micrite cements of the larger nodules in the paleosol profile cluster at –8.6 and –5.4 (Table 1). As established in previous work (Tabor et al. 2007; Gastaldo et al. 2014), large differences of $\delta^{13}C$ between calcite and organic matter (OM) indicate that soil development occurred under well-drained conditions at the time of calcite-cement genesis and nodule formation (Gastaldo et al. 2014). The

TABLE 2.—*Weight% of calcium carbonate, $\delta^{13}C$ (‰VPDB), standard deviation of ^{13}C, $\delta^{18}O$ (‰VPDB), and the standard deviation of ^{18}O obtained from micritic calcite. Nodules collected at a depth of 70 cm were analyzed at their centers and peripheries to ensure whether the genesis of septarian cracks had altered their signature.*

Sample ID	Weight% CC	$\delta^{13}C$ (‰VPDB)	$\delta^{13}C$ Std Dev	$\delta^{18}O$ (‰VPDB)	$\delta^{18}O$ Std Dev	^{18}O (‰VSMOW)
280517.3 nodule	25	–8.62	0.007	–21.24	0.007	9.02
280517.8 nodule center	59	–8.08	0.013	–21.24	0.031	9.02
280517.8 nodule periphery	64	–5.49	0.009	–21.71	0.013	8.54
280517.8 nodule periphery R	62	–5.49	0.016	–21.67	0.004	8.58
Lower calcic paleosol	57	–5.44	0.021	–21.71	0.02	8.54
Upper calcic paleosol	60	–5.58	0.005	–21.59	0.043	8.66

TABLE 3.—*Molecular weathering proxies, Chemical Index of Alteration minus potassium (CIA-K), CALMAG, estimates of mean annual precipitation (MAP) using CIA-K and CALMAG, and estimate of mean annual temperature (MAT). Bt horizon was identified using the positive CIA-K excursion at a depth of 80 cm.*

Depth in Profile (m)	Base Loss				Clayeyness	Mineral Assemblage Stability	Calcification	Salinization	Mineral Maturity	molar ratio					
	Na/Ti	Ca/Ti	K/Ti	Mg/Ti	Al/Si	Fe/K	(Ca+Mg)/Al	(K+Na)/Al	Si/Al	Al / (Al+Ca+Na+K)	CALMAG	CIA-K	MAP: CALMAG	MAP: CIA-K	MAT
0	7.68	5.67	4.44	6.70	0.12	0.68	0.54	0.53	8.64	56.40	65.03	63.28	1039.74	768.83	7.56
–0.1	4.77	7.10	5.07	6.90	0.13	0.80	0.66	0.47	7.64	55.48	60.14	64.01	928.69	779.88	8.67
–0.2	4.43	9.17	5.31	6.69	0.13	0.83	0.75	0.46	7.58	52.79	57.14	60.87	860.69	733.06	8.78
–0.3	4.49	6.23	5.29	6.17	0.13	0.83	0.59	0.46	7.56	56.79	62.94	66.26	992.22	815.23	8.70
–0.4	4.11	13.17	5.62	6.36	0.14	0.80	0.93	0.46	7.13	47.92	51.90	54.94	741.75	652.23	8.76
–0.5	4.24	7.33	5.64	6.13	0.14	0.78	0.64	0.47	7.34	55.13	61.13	64.64	951.13	789.65	8.66
–0.6	4.05	8.60	5.34	6.22	0.14	0.89	0.74	0.47	7.23	52.82	57.61	61.43	871.29	741.21	8.67
–0.7	4.85	4.48	5.89	5.91	0.14	0.75	0.47	0.49	7.26	59.04	67.86	70.16	1104.02	880.29	8.24
–0.8	4.39	4.55	6.06	5.74	0.14	0.73	0.48	0.48	6.96	59.01	67.73	70.72	1100.91	890.09	8.35
–0.9	6.37	5.13	5.41	4.97	0.13	0.70	0.46	0.53	7.68	56.56	68.55	65.69	1119.59	806.11	7.41
–1	5.82	4.55	5.32	5.13	0.13	0.74	0.46	0.53	7.46	57.14	68.35	66.84	1115.16	824.62	7.45
–1.1	6.23	1.93	5.52	4.86	0.13	0.70	0.31	0.54	7.49	60.62	73.92	71.64	1241.52	897.60	7.25
–1.2	4.84	2.24	4.39	5.00	0.13	0.87	0.39	0.49	7.89	62.04	72.14	72.59	1200.95	923.53	8.19
–1.3	5.24	2.87	4.99	5.10	0.14	0.83	0.40	0.51	7.13	60.61	71.67	71.31	1190.35	900.54	7.91

observed variability is large and, likely, corresponds to variable water availability and biological soil activity. Both processes affect the $\delta^{13}C$ of soil CO_2 and corresponding $\delta^{13}C$ values of calcite through time. A similar set of values was reported by Gastaldo et al. (2014) for a short concretion-bearing interval at NWP that sits stratigraphically higher than those in the 527/Quaggasfontein–Pienaarsbaken section (Fig. 11). These NWP values are in contrast to more negative values throughout the rest of that section, many of which are indicative of a methanogenic origin in waterlogged conditions for the micrite cement (Tabor et al. 2007). The presence of *Katbergia* burrows in other coeval localities, along with $\delta^{13}C$ values of micrite cement in entombing nodules, are interpreted to reflect more water-saturated pore spaces at the time of invertebrate colonization and burrowing activity. Hence, the conditions under which the gleyed calcic Vertisol formed appear to have been polygenetic, and these paleosols are interpreted as compound or composite soils (*sensu* Marriott and Wright 1993). They reflect an aggradational and degradational history (Gastaldo and Demko 2011) characterized by variable drainage conditions from poorly drained to better drained during their formation.

Based on field observations and data acquired, we envision the mechanisms and processes responsible for the formation of this soil, and probably others in the 527/Quaggasfontein succession, to be part of a five-step depositional and weathering process (Fig. 12). The stratigraphic stacking patterns appear to begin with deposition of overbank fines on the floodplain that are associated with plant debris in poorly drained conditions conducive to preservation of organic matter (DiMichele and Gastaldo 2008; Fig. 12A). Crosscutting relationships of ichnotaxa and rooting demonstrate a slight improvement of drainage that allow for the colonization by burrowing invertebrates and stabilization by plants, pioneered into a newly established better, but variably drained, landscape. This condition is evidenced by *Katbergia* burrows at the exclusion of fossilized plant debris (Fig. 12B) and represents the initial episode of pedogenesis associated with the lower parts of the paleosol. The incipient stages ceased as burrow backfilling and poor drainage continued (Fig. 12C). Petrographic observations of weathered materials (opaques) and substantially higher %LOI values from 30 to 80 cm, paralleling a trend in phyllosilicates, indicates a second episode of downcutting, a lowering of the water table, and improved drainage conducive to down-profile translocation of fine-grained materials (i.e., argillic Bt horizon). Furthermore, these improved drainage conditions also translocated Ca^{2+} in conjunction with clays down the soil profile, allow for the precipitation of calcite cements (Btk; Fig. 12D).

A common feature of Alfisols and other soils with argillic horizons in bottomland settings is a trend toward poorer drainage due to reduced permeability and porosity in the argillic horizon. This commonly leads to pedoturbation, the formation of slickensides, and development of vertic-type morphologies. Hence, we envision the final phase of pedogenesis to be associated with the return of a higher local or regional water table, and formation of a near-surface Bkss horizon. Under these conditions, slickensides develop in association with the pre-existing upper parts of an argillic horizon (e.g., Weitkamp et al. 1996) along with renewed carbonate precipitation (Fig. 12E). This succession of events describes the complicated processes and mechanisms of a single profile, one of seven recognized in this stratigraphy (Fig. 3).

It is important to note that the interpretation of variable drainage is supported by lateral facies relationships and stratigraphic variability that demonstrates incision, channelization, and backfilling of an equivalent thickness to the interval in which a succession of calcic Vertisols is preserved. We also emphasize that substantially improved drainage occurred across the interfluves during incision and channelization of the largest channel (Fig. 3). This was a period during which improved drainage promoted the formation of argillic soil horizons. It is possible that each paleosol profile has a major channel-incision phase associated with it. Collectively, the scenario outlined here explains the trends observed in profile-scale elemental ratios, CIA-K and CALMAG trends, LOI, and $\delta^{13}C$ data.

Comparison with Previous Paleoclimate Interpretations

Smith (1995) emphasizes several paleosol features of the *Lystrosaurus* Assemblage Zone that are indicative of modern calcretes. These include the presence of calcareous nodules and nodular horizons, along with carbonate-enriched desiccation cracks, all of which are interpreted to be indicative of warm, semiarid conditions. Estimates for both MAT (16–20° C) and a highly seasonal rainfall (100–700 mm/yr) are reported in Smith (1995) based on observations reported in Reeves (1976) and Semeniuk and Searle (1985), respectively.

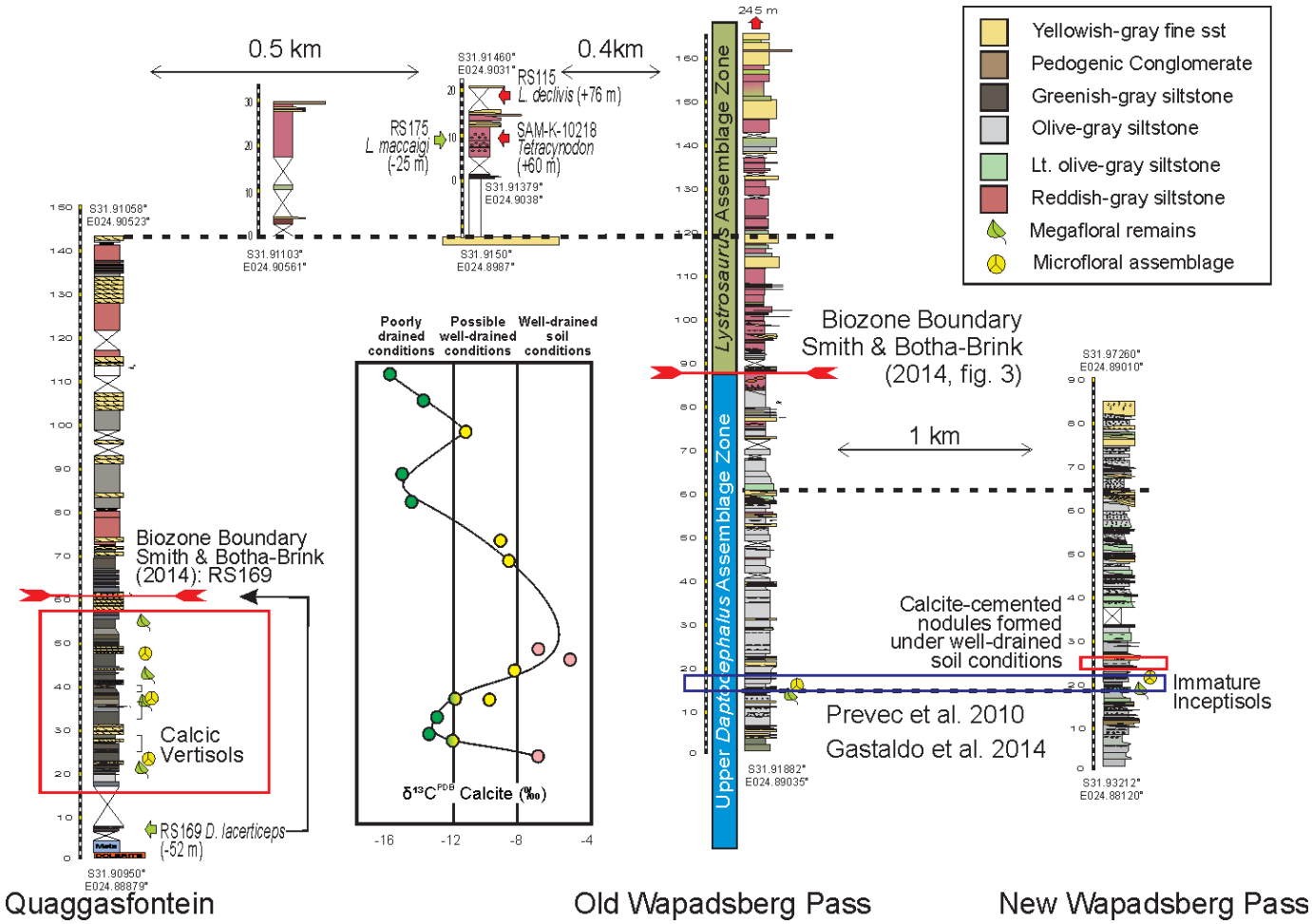

FIG. 11.—Physical correlation of the measured sections in the area. The physical correlation between the 527/Quaggasfontein and Old Wapadsberg Pass sections uses a prominent sandstone bench at a stratigraphic position of ~ 135 m, which can be physically walked (traced) for 0.9 km, into the *Lystrosaurus* Assemblage Zone. This correlation was augmented by measuring the vertical stratigraphic distance between the sandstone bench and boundary proposed by Smith and Botha-Brink (2014). Note the discrepancy in: 1) the stratigraphic position of the assemblage-zone boundary (= PTB; Ward et al. 2000, 2005; Smith and Botha-Brink 2014) based on RS169 (*D. laceriteps*), the reported position of which is 52 m below it, and the placement of that boundary in the OWP section (Ward et al. 2000, 2005; Smith and Ward 2001; Smith and Botha-Brink 2014); 2) the occurrence of the *Daptocephalus* Assemblage Zone taxon, *L. maccaigi* (RS175) reported by Smith and Botha-Brink (2014) at a stratigraphic position 25 m below the boundary, approximately 50 m into the *Lystrosaurus* AZ; and 3) the disparity in the reported (values in brackets) and actual stratigraphic positions of *Tetracynodon* (SAM-K-10218) and *L. declivis* (RS115). We note that all three of these specimens are reported to have been collected from an area with little local topographic relief. The correlation between OWP and NWP is that documented by Gastaldo et al. (2014) which, in part, is based on the occurrence of stacked Protosols in which Prevec et al. (2010) report a well-preserved *Glossopteris* flora of late Chanhsingian age. A $\delta^{13}C$ curve, based on values obtained from *in situ* carbonate-cemented nodules from the Quaggasfontein (current study), Old and New Wapadsberg Pass sections (Gastaldo et al. 2014), identifies at least two, and possibly three, oscillations in drainage, interpreted in response to climate, during the upper *Daptocephalus* Assemblage Zone. Stratigraphic column scale in meters.

It is unclear from these references as how climate constraints were determined for *Lystrosaurus* Assemblage Zone calcic paleosols by Smith (1995). Reeves (1976) describes the Quaternary deposits of the Southern High Plains, defined by the presence of a caliche "caprock" of the Ogallala Formation, which extends across parts of Texas and New Mexico, USA. Aridification in these Quaternary deposits is exhibited by: 1) well developed B horizons above Cca (or BCk) horizons in the "Sangamon Soil"; in the Wisconsinan paleosurfaces 2) the presence of gypsum and carbonate-cemented lenses in the Tahokan deposits associated with shoreline lake deposits; and 3) small epsomite-and-gypsum crystals and occasional rosettes in the Double Lakes Formation. Reeves (1976, p. 223) interprets an overall semiarid climate in which the area "perhaps" experienced wetter intervals or phases. The only discussion of temperature pertains to his estimate of a 10° C cooler mean summer temperature during the last full glacial episode, and precipitation estimated at 38″/yr (950 mm/yr) during the last full glacial. These values were derived from sediment cores recovered in small, closed basins (Reeves 1976, p. 225). Earlier, Reeves (1970) noted that the present extent of calcic soils is marked by the ~ 25″/yr (625 mm/yr) rainfall line with a MAT of 60° F (15.6° C) in the area. Semeniuk and Searle (1985) describe Holocene calcrete soils in relation to subtropical to semiarid climates along the coastal plain of southwestern Australia. Here, MAT varies from 21° to 23° C, and is accompanied by a precipitation regime ranging from 480 mm/yr to 990 mm/yr (Semeniuk and Searle 1985, their Table 1). As such, we assert that only current MAT and MAP estimates provided herein can be considered reliable for the interval spanning the *Daptocephalus–Lystrosaurus* AZ boundary.

The distribution of paleosol types, along with the stable-isotope geochemical trends, in the Wapadsberg Pass area demonstrate episodic changes in drainage, interpreted to reflect the influence of climate, in the

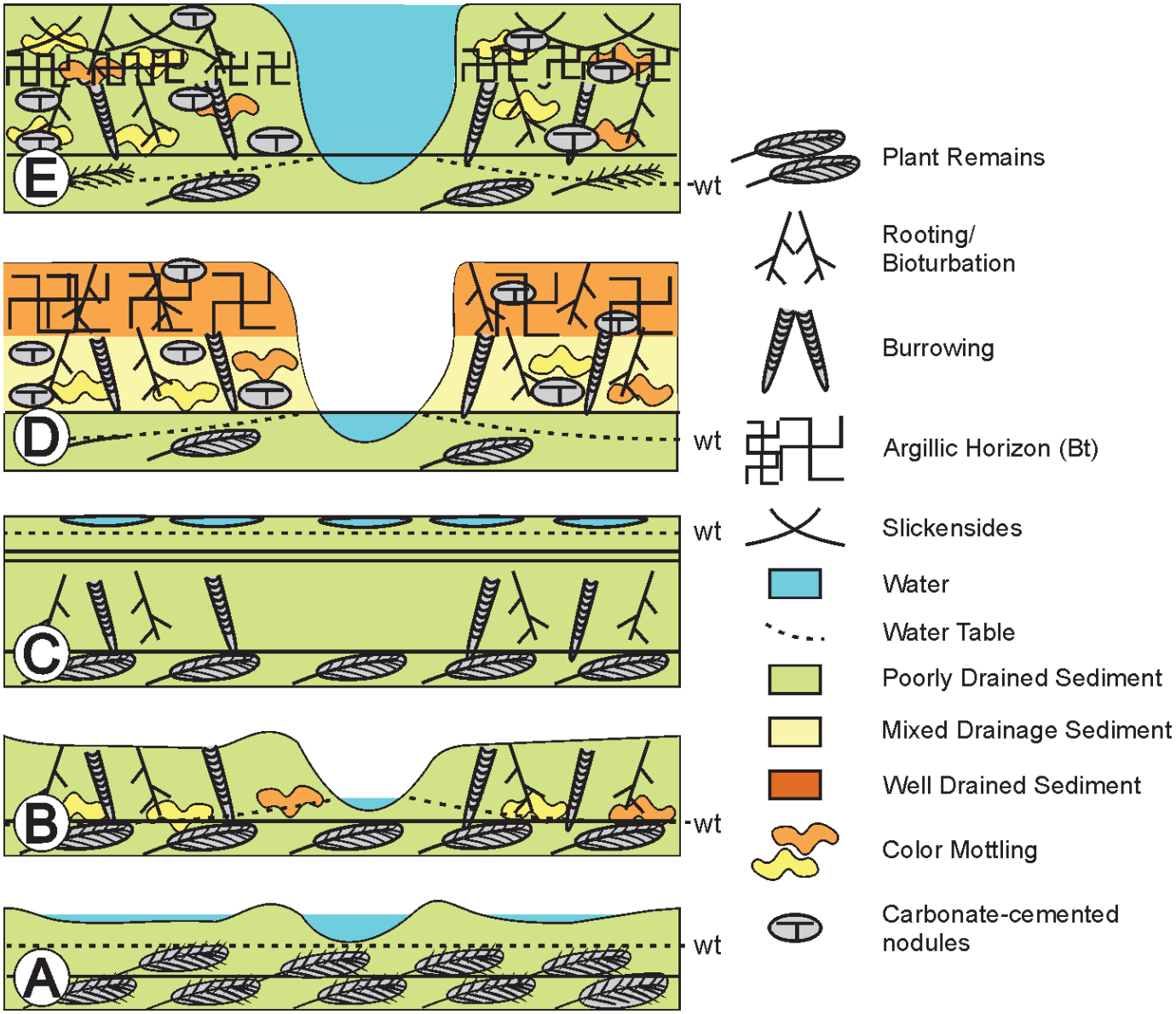

FIG. 12.—Mechanistic, process-based model for the formation of paleosols in the Quaggasfontein stratigraphic succession. **A)** Pre-pedogenesis deposition of siltstones and associated fossil-plant organic matter in relatively quiet, slack-water environments, such as mini-basins or palustrine ponds across the fluvial floodplains under poorly drained conditions. **B)** Subsequent lowering of the water table leads to variable, but overall improved, drainage permissive of colonization by burrowing aerobic organisms (*Katbergia* ichnofossil) as well as rooting plants that, at least, partially disturb sedimentary bedding leading to the destruction of previously buried organic matter and, perhaps, some color mottling associated with redistribution and concentration of Fe and Mn oxides. **C)** A return to poor drainage, backfilling of channels, and overbank sedimentation results in a cessation of incipient pedogenesis associated with development of phase (B). **D)** Another regional drop in groundwater table, associated with a change in fluvial gradient, leads to incision of fluvial channels and better drainage across the interfluvial floodplains. During this episode of downcutting, free drainage within the interfluvial soils permits vertical, piston flow of precipitation and down-profile translocation of fine materials leading to formation of an argillic (Bt) horizon and leaching of Ca^{2+} to form horizons of subsurface carbonate cements (Bk). **E)** Formation of a thick argillic horizon reduces permeability and porosity over time and, in conjunction with a rising water table and eventual burial of the soils, results in a final phase of poor drainage. This phase results in the reworking of the upper parts of the argillic horizon into slickensided soil materials (Bss) through the process of pedoturbation.

late Changhsingian (Fig. 11). Using stable oxygen- and carbon-isotope data obtained from bone and teeth, Rey et al. (2016) also interpret a change in climate during the Late Permian, albeit on much longer timescales. They propose that a slight decrease in continental $\delta^{18}O_p$ V-SMOW values across the Capitanian–Wuchiapingian equates to a drop in temperature ranging between 3 ± 9° and 3.5 ± 11° C. They equate this trend to correspond with the global signal in the marine record of the end-Capitanian event with a question mark (Rey et al. 2016, their Fig. 4). The Capitanian–Wuchiapingian trend is accompanied by a negative shift in values for $\delta^{13}C$ V-PDB through this interval, from –10‰ to –31‰, with the most negative average value at the top of the *Cistecephalus* Assemblage Zone (N = 3; Rey et al. 2016, their supplemental data Table 1). The trend in $\delta^{13}C$ values becomes more positive in the Lower *Daptocephalus* AZ where the average value is reported to be –13.5‰ (N = 6), whereas the average $\delta^{13}C$ value obtained from bone in the Upper *Daptocephalus* AZ is reported to decrease to near –16‰. The latter value represents a minimum based on a

single sample (PV/GD17, *Dicynodon* sp. collected from the Elandsberg Member at Inhoek; Rey et al. 2016, their supplemental data Table 1). We note, though, that their data indicate an average value for all specimens of –14‰ and an average value of –12.5‰ for all therapsids when the two additional Upper *Daptocephalus* AZ samples are included in the calculation (N = 3 ± 4.2‰). The most positive value reported from bone from this very small data set is –7.7‰, which falls within our $\delta^{13}C$ values obtained from calcite-cemented nodules (Table 2). We also note that average $\delta^{13}C$ values in the *Daptocephalus* AZ are not much different from values in the overlying *Lystrosaurus* AZ (–13.3‰ for all taxa, –13.1‰ for therapsids).

Two $\delta^{18}O_p$ values are plotted by Rey et al. (2016) in the Upper *Daptocephalus* AZ, both of which are ~ 3‰, and the trend is described as an abrupt shift of 8‰ from the Lower *Daptocephalus* AZ (although plotted as an ~ 5‰ shift; their Fig. 4). These values represent only two (PV/GD14 Therapsidan, PV/GD17 *Dicynodon*) of the three reported in the supplemental data set; the $\delta^{18}O_p$ value of the third sample (PV/GD11 *Daptocephalus*) is 4.5‰. When averaged, the $\delta^{18}O_p$ value for the Upper *Daptocephalus* AZ is 3.7‰, which results in a shift of an ~ 4‰ (based on a very limited data set). Using these oxygen-isotope records, Rey et al. (2016) interpret an abrupt and significant warming of 17 ± 5° C at the "boundary." From whence the three samples originate in the stratigraphy, other than somewhere in the Upper *Daptocephalus*, is unknown. Two samples were collected at Inhoek (one each from the Palingkloof and Elandsberg members), whereas the third sample comes from Schalkwykskraal (Elandsberg Mbr. adjacent to the Gariep Dam reservoir in the Eastern Cape Province); neither of these stratigraphic sections have been described or published, nor have any correlations been made to more "classic" sections in the area.

Trends in Late Permian Drainage

The *Daptocephalus* Assemblage Zone is subdivided into lower and upper zones by Viglietti et al. (2016), where the uppermost ~ 170 m is reportedly characterized by the absence of *Dicynodon* (but see Gastaldo et al. 2015, 2017, 2019b) and the continuation of *Daptocephalus*, which, in turn, is overlain by the *Lystrosaurus* Assemblage Zone (Figs. 1, 3). The exact position of the latter faunal turnover is ambiguous (Gastaldo et al. 2015, 2017, 2019b; Neveling et al. 2016), and Smith and Botha-Brink's (2014) vertebrate data at Old Wapadsberg Pass offer no clarification on the question (Fig. 11). Nevertheless, physical correlation of the 527/Quaggasfontein stratigraphy with Old Wapadsberg and New Wapadsberg passes (Gastaldo et al. 2014; supplemental data) demonstrate that the calcic Vertisol interval lies > 90 m below the horizon at which Smith and Botha-Brink (2014, their Fig. 3c) place the biozone boundary at Old Wapadsberg Pass. These soils also lie stratigraphically near the paleosol interval reported by Gastaldo et al. (2014) in which an autochthonous *Glossopteris* flora is preserved (Prevec et al. 2010). The stable-isotope $\delta^{13}C$ values from calcite-cemented nodules at Quaggasfontein indicate that micrite cements in these concretions precipitated under well-drained conditions below to the immature Inceptisols stratigraphically higher at Wapadsberg Pass (Fig. 11). Gastaldo et al. (2014, their Fig. 9) report in outcrops along the R61 highway that an interval of nodules in which the calcite $\delta^{13}C$ values are too negative for cement to have precipitated under well-drained conditions. These nodules are overlain, within 15 m, by two closely spaced nodular horizons where the $\delta^{13}C$ values reflect well-drained conditions. $\delta^{13}C$ values stratigraphically above these two horizons exhibit a unidirectional trend towards poorly drained soils and methanogenic-derived cements (Fig. 11). Hence, with the available data, there appear to be at least two, and possibly three, changes in the drainage of this part of the *Daptocephalus* AZ soils, interpreted to reflect climate cycles recorded ~ 120 m beneath the reported turnover in vertebrate assemblage zones at Wapadsberg Pass. Vegetation grew under cool to cold conditions, accompanied by a seasonal rainfall regime and development of stage II calcic Vertisols (Machette 1985), and periods when soil conditions were more waterlogged, providing for the establishment of glossopterid forests. The recognition of these shifts in the latest Chanhsinghian is in contrast with interpretations of rapid and unidirectional aridification under hot-and-dry conditions (e.g., Ward et al. 2005; MacLeod et al. 2017). The significance of this difference in interpreted paleoclimatic conditions cannot be overstated. Very different interpreted patterns are the result of coarse geochemical studies presented in a generalized composite stratigraphy when compared with those undertaken within a high-resolution stratigraphic framework. A unidirectional climate shift connotes a more stable trend than the disturbed variance in water availability that appears to emerge from more detailed scrutiny of the lithostratigraphy and its geochemical trends in the Upper *Daptocephalus* Assemblage Zone.

CONCLUSIONS

The development of calcic paleosols in the latest Permian of the Karoo Basin, before a reported turnover in vertebrate fauna, has been inferred from the presence of calcite-cemented pedogenic nodules concentrated in fluvial channel-lag deposits. These are first encountered in the Elandsberg Member (Gastaldo et al. 2018) and become more common higher in the Katberg Formation (Pace et al. 2009; Neveling et al. 2016). Yet, to date, physical evidence for their occurrence has been elusive, primarily because of multiple episodes of landscape degradation that characterizes this interval (Gastaldo and Demko 2011; Gastaldo et al. 2015, 2018). Exposures of the upper *Daptocephalus* Assemblage Zone adjacent to an erosional channel fill on farm Quaggasfontein, and ~ 120 m below the vertebrate biozone boundary in the Old Wapadsberg Pass area, offer the first insights into not only the formation of these soils, but also into the prevailing climate conditions under which they developed.

Stage II, calcic Vertisol intervals are characterized by an array of pedogenic features previously reported for Upper Beaufort Group paleosols. These include a soil matrix of greenish-gray siltstone, which may be reddish-gray mottled, accompanied by slickensides and small, scattered calcareous nodules, or nodular horizons, some of which may show septarian shrinkage cracks. There are several unique characteristics of these soils not reported previously. *Katbergia* burrows, interpreted as having been excavated by decapod-crustaceans (Gastaldo and Rolerson 2008), are common in the lowermost ~ 30 cm of soils above unaltered C horizons in which primary structures are preserved. Where the burrowed interval is absent, adpressions of robust plant debris are preserved. Micromorphology shows that many pedogenically altered layers are characterized by single-grain structure. Isolated, euhedral pyrite crystals are seen in thin section, and coeval Wuchiapingian volcanisms may have been the source for increased sulfur into the landscape. Erosion of these soils under a change in climate regime accounts for the presence of euhedral pyrite grains along bedding planes of crossbed sets in coeval fluvial channel deposits.

Whole-rock geochemical analyses of one calcic Vertisol profile demonstrate two phases of development. The older and basalmost interval in which either *Katbergia* burrows or plant detritus occurs exhibits no down-profile trend in elemental values. In contrast, elemental values in the younger and upper soil, in which calcite-cemented nodules of varying sizes are most common, do exhibit down-profile trends. CIA-K values of sampled horizons range from 55 near the top to 72 near the bottom and, in combination, are used to interpret a polygenetic origin for the paleosol. Stable-isotope values of $\delta^{13}C$, obtained from micrite cements in larger nodules, indicate that these cements precipitated under well-drained conditions characterized by open-system gaseous exchange with the overlying Permian atmosphere. Micrite cements were not a product of anoxia and closed-system methanogenesis in soils characterized by undersaturated pore waters, or waterlogged conditions. Estimates of

MAT and MAP indicate that the prevailing climate at the time of pedogenesis was seasonally cold (MAT = 10.2 ± 4.4° C) and humid (MAP = 1083 ± 181 mm/year). Physical correlation of the stratigraphic section at 527/Quaggasfontein and $\delta^{13}C$ values from our previously published stratigraphies at Old Wapadsberg and New Wapadsberg passes (Gastaldo et al. 2014) indicate that the Late Permian landscape experienced episodically wet and episodically dry phases that alternated. Conditions under which these soils formed are interpreted to reflect differences in the prevailing climate. Hence, there is an overall wetting trend in the Wapadsberg Pass region towards the *Daptocephalus–Lystrosaurus* Assemblage Zone boundary, which is used by several workers to mark the end-Permian crisis that is reported to have rapidly occurred under dry and hyperarid conditions. There is no evidence in the Wapadsberg Pass area to support this narrative.

SUPPLEMENTAL MATERIAL

https://www.sepm.org/supplemental-materials

ACKNOWLEDGMENTS

The authors would like to thank the following colleagues for field assistance: Ms. Sisanda Makubalo, Council for Geoscience, Pretoria, and Mr. Samuel Sinkler, Colby College. We acknowledge the long relationship we have with the following individuals who have given us permission to work on their farms: Pieter Locke and Jaco Loots. Research efforts were supported, in part, by the Council for Geoscience (South Africa), National Science Foundation EAR 0417317, EAR 1123570, and EAR 1624302, and a Fulbright Research Fellowship to RAG. The authors appreciated the constructive comments by two anonymous reviewers of a previous manuscript draft, and Drs. Erik Gulbranson and Greg Ludvigson, which have improved the final manuscript.

REFERENCES

Abbott, P.L., Minch, J.A., and Peterson, G.L., 1976, Pre-Eocene paleosol south of Tijuana, Baja California, Mexico: Journal of Sedimentary Petrology, v. 46, p. 355–361.

Benton, M.J., and Newell, A.J., 2014, Impacts of global warming on Permo-Triassic terrestrial ecosystems: Gondwana Research, v. 25, p. 1308–1337, doi:10.1016/j.gr.2012.12.010.

Blewett, S.C.J., and Phillips, D., 2016, An overview of Cape Fold Belt geochronology: implications for sediment provenance and the timing of orogenesis, *in* Linol, B., and de Wit, M., eds., Origin and Evolution of the Cape Mountains and Karoo Basin: Springer, Regional Geology Reviews, p. 49–55.

Botha-Brink, J., Huttenlocker, A.K., and Modesto, S.P., 2014, Vertebrate paleontology of Nooitgedacht 68: a *Lystrosaurus maccaigi*-rich Permo-Triassic Boundary locality in South Africa, *in* Kammerer, C.F., Angielczyk, K.D., and Fröbisch, J., eds., Early Evolutionary History of the Synapsida, Vertebrate Paleobiology and Paleoanthropology: Dordrecht, Springer, p. 289–304, doi:10.1007/978-94-007-6841-3_17.

Bown, T.A., and Kraus, M., 1987, Integration of channel and floodplain suites: developmental sequence and lateral relations of alluvial paleosols: Journal of Sedimentary Petrology, v. 57, p. 587–601.

Brewer, R.C., 1964, Fabric and Mineral Analysis of Soils: New York, Wiley, 470 p.

Brimhall, G.H., Lewis, C.J., Ague, J.J., Dietrich, W.E., Hampel, J., Teague, T., and Rix, P., 1988, Metal enrichment in bauxites by deposition of chemically mature aeolian dust: Nature, v. 333, p. 819–824.

Brimhall, G.H., Lewis, C.J., Ford, C., Bratt, J., Taylor, G., and Warin, O., 1991a, Quantitative geochemical approach to pedogenesis: importance of parent material reduction, volumetric expansion, and eolian influx in laterization: Geoderma, v. 51, p. 51–91.

Brimhall, G.H., Chadwick, O.A., Lewis, C.J., Compston, W., Williams, I.S., Danti, K.J., Dietrich, W.E., Power, M., Hendricks, D., and Bratt, J., 1991b, Deformational mass transfer and invasive processes in soil evolution: Science, v. 255, p. 695–702.

Broom, R., 1906, On the Permian and Triassic faunas of South Africa: Geological Magazine, Decade, v. 5, p. 29–30.

Broom, R., 1911, On some new South African Permian reptiles: Zoological Society of London, Proceedings, p. 1073–1082.

Burgess, S.D., and Bowring, S., 2015, High-precision geochronology confirms voluminous magmatism before, during, and after Earth's most severe extinction: Science Advances, v. 1, doi:10.1126/sciadv.1500470.

Burgess, S.D., Bowring, S., and Shen., S., 2014, High-precision timeline for Earth's most severe extinction: National Academy of Science (USA), Proceedings, v. 111, p. 3316–3321.

Capo, R., Whipkey, C.E., Blachere, J.R., and Chadwick, O.A., 2000, Pedogenic origin of dolomite in a basaltic weathering profile, Kohala Peninsula, Hawaii: Geology, v. 28, p. 271–274.

Catuneanu, O., Wopfner, H., Eriksson, P.G., Cairncross, B., Rubidge, B.S., Smith, R.M.H., and Hancox, P.J., 2005, The Karoo basins of south-central Africa: Journal of African Earth Sciences, v. 43, p. 211–253.

Caudill, M.R., Driese, S.G., and Mora, C.I., 1996, Preservation of a paleo-Vertisol and an estimate of late Mississippian paleoprecipitation: Journal of Sedimentary Research, v. 66, p. 58–70.

Caudill, M.R., Driese, S.G., and Mora, C.I., 2008, Physical comparison of vertic palaeosols: implications for burial diagenesis and palaeo-precipitation estimates: Sedimentology, v. 44, p. 673–685.

Coney, L., Reimold, W.U., Hancox, P.J., Mader, D., Koeberl, C., McDonald, I., Struck, U., Vajda, V., and Kamo, S., 2007, Geochemical and mineralogical investigation of the Permian–Triassic boundary in the continental realm of the southern Karoo Basin, South Africa: Palaeoworld, v. 16, p. 67–104.

Craig, H., 1957, Isotopic standards for carbon and oxygen and correction factors for mass-spectrometric analysis of carbon dioxide: Geochimica et Cosmochimica Acta, v. 12, p. 133–149.

Cui, Y., and Kump, L.R., 2014, Global warming and the end-Permian extinction event: proxy and modeling perspectives: Earth-Science Reviews, v. 149, p. 5–22, doi:10.1016/j.earscirev.2014.04.007.

DiMichele, W.A., and Gastaldo, R.A., 2008, Plant paleoecology in deep time: Missouri Botanical Gardens, Annals, v. 95, p. 144–198.

Driese, S.G., Mora, C.I., Stiles, C.A., Joeckel, R.M., and Nordt, L.C., 2000, Mass-balance reconstruction of a modern Vertisol: implications for interpreting the geochemistry and burial alteration of paleo-Vertisols, Geoderma, v. 95, p. 179–204.

Driese, S.G., Nordt, L.C., Lynn, W.C., Stiles, C.A., Mora, C.I., and Wildings, L.P., 2005, Distinguishing climate in the soil record using chemical trends in a Vertisol climosequence from the Texas coast prairie, and application to interpreting Paleozoic paleosols in the Appalachian Basin, U.S.A.: Journal of Sedimentary Research, v. 65, p. 339–349.

Feng, W., and Yapp, C.J., 2009, Paleoenvironmental implications of concentration and $^{13}C/^{12}C$ ratios of $Fe(CO_3)OH$ in goethite from a mid-latitude Cenomanian laterite in southwestern Minnesota: Geochimica et Cosmochimica Acta, v. 73, p. 2559–2580.

Gastaldo, R.A., and Demko, T.M., 2011, The relationship between continental landscape evolution and the plant-fossil record: long term hydrology controls that plan fossil record, *in* Allison, P.A., and Bottjer, D.J., eds., Taphonomy, Second Edition: Processes and Bias Through Time: Springer, The Netherlands, Topics in Geobiology, v. 32, p. 249–286.

Gastaldo, R.A., and Neveling, J., 2016, Comment on: "Anatomy of a mass extinction: Sedimentological and taphonomic evidence for drought-induced die-offs at the Permo-Triassic boundary in the main Karoo Basin, South Africa": Palaeogeography, Palaeoclimatology, Palaeoecology, v. 396, p. 99–118, doi:10.1016/j.palaeo.2014.01.002.

Gastaldo, R.A., and Rolerson, M.W., 2008, *Katbergia* gen. nov., A new trace fossil from the Upper Permian and Lower Triassic rocks of the Karoo Basin: implications for paleoenvironmental conditions at the P/Tr extinction event: Palaeontology, v. 51, p. 215–229.

Gastaldo, R.A., Adendorff, R., Bamford, M.K., Labandeira, C.C., Neveling, J., and Sims, H.J., 2005, Taphonomic trends of macrofloral assemblages across the Permian–Triassic boundary, Karoo Basin, South Africa: Palaios, v. 20, p. 478–497.

Gastaldo, R.A., Neveling, J., Clark, K., and Newbury, S.S., 2009, The terrestrial Permian–Triassic boundary event bed is a non-event: Geology, v. 37, p. 199–202.

Gastaldo, R.A., Pludow, B.A., and Neveling, J., 2013, Mud aggregates from the Katberg Formation, South Africa: additional evidence for Early Triassic degradational landscapes: Journal of Sedimentary Research, v. 83, p. 531–540.

Gastaldo, R.A., Knight, C.L., Neveling, J., and Tabor, N.J., 2014, Latest Permian paleosols from Wapadsberg Pass, South Africa: implications for Changhsingian climate: Geological Society of America, Bulletin, v. 126, p. 665–679, doi:10.1130/B30887.1.

Gastaldo, R.A., Kamo, S.L., Neveling, J., Geissman, J.W., Bamford, M., and Looy, C.V., 2015, Is the vertebrate defined Permian–Triassic Boundary in the Karoo Basin, South Africa, the terrestrial expression of the End Permian marine event?: Geology, v. 43, p. 939–942, doi:10.1130/G37040.1.

Gastaldo, R.A., Neveling, J., Looy, C.V., Bamford, M.K., Kamo, S.L., and Geissman, J.W., 2017, Paleontology of the Blaauwater 67 Farm, South Africa: testing the *Daptocephalus/Lystrosaurus* Biozone Boundary in a Stratigraphic Framework: Palaios, v. 34, p. 349–366, doi:10.2110/palo.2016.106.

Gastaldo, R.A., Neveling, J., Geissman, J.W., and Kamo, S.L., 2018, A lithostratigraphic and magnetostratigraphic framework in a geochronologic context for a purported Permian–Triassic boundary section at Old (West) Lootsberg Pass, Karoo Basin, South Africa: Geological Society of America, Bulletin, v. 130, p. 1411–1438, doi:10.1130/B31881.1.

Gastaldo, R.A., Neveling, J., Geissman, J.W., and Li., J.W., 2019a, A multidisciplinary approach to review the vertical and lateral facies relationships of the purported vertebrate-defined terrestrial boundary interval at Bethulie, Karoo Basin, South Africa: Earth Science Reviews, v. 189, p. 220–243, doi:10.1016/j.earscirev.2017.08.002.

Gastaldo, R.A., Neveling, J., Geissman, J.W., and Looy, C.V., 2019b, Testing the *Daptocephalus* and *Lystrosaurus* Assemblage Zones in a lithostratographic, magneto-

stratigraphic, and palynological framework in the Free State, South Africa: Palaios, v. 34, p. 542–561, doi:10.2110/palo.2019.019.

Gastaldo, R.A., Kamo, S.L., Neveling, J., Geissman, J., Looy, C.V., and Martini, A.M., 2020, The base of the *Lystrosaurus* Assemblage Zone, Karoo Basin, predates the end-Permian marine extinction: Nature Communications, doi: https://doi.org/10.1038/s41467-020-15243-7.

Gill, S., and Yemane, K., 1996, Implications of a Lower Pennsylvanian Ultisol for equatorial Pangean climates and early, oligotrophic, forest ecosystems: Geology, v. 24, p. 905–908.

Gonfiantini, R., 1984, Stable isotope reference samples for geochemical and hydrological investigations: The International Journal of Applied Radiation and Isotopes, v. 35, p. 426

Gulbranson, E.L., Tabot, N.J., and Montañez, I.P., 2011, A pedogenic record of soil CO_2 variations as a response to soil moisture content: Geochimica et Cosmochimica Acta, v. 75, p. 709–7116.

Heydari, E., Hassandzadeh, J., and Wade, W.J., 2000, Geochemistry of central Tethyan upper Permian and lower Triassic strata, Abadeh region, Iran: Sedimentary Geology, v. 137, p. 85–99.

Hotinski, R.M., Bice, K.L., Kump, L.R., Najjar, R.G., and Arthur, M.A., 2001, Ocean stagnation and end-Permian anoxia: Geology, v. 29, p. 7–10.

Hsieh, J.C.C., and Yapp, C.J., 1999, Stable carbon isotope budget of CO_2 in a wet, modern soil as inferred from $Fe(CO_3)OH$ in pedogenic goethite: possible role of calcite dissolution: Geochimica et Cosmochimica Acta, v. 63, p. 767–783.

Isbell, J., Cole, D.I., and Catuneau, O., 2008, Carboniferous–Permian glaciation in the main Karoo Basin, South Africa: stratigraphy, depositional controls, and glacial dynamics, *in* Fielding, C.R., Frank, T.D., and Isbell, J.L., eds., Resolving the Late Paleozoic Gondwanan Ice Age in Time and Space: Geological Society of America, Special Paper 441, p. 71–82.

Johnson, M.R., van Vuuren, C.J., Visser, J.N.J., Cole, D.I., Wickens, H.D., Christie, A.D.M., Roberts, D.L., and Brandl, G., 2006, Sedimentary rocks of the Karoo Supergroup, *in* Johnson, M.R., Anhaeusserm, C.R., and Thomas, R.J., eds., The Geology of South Africa: Johannesburg, Geological Society of South Africa, Council for Geoscience, p. 461–479, 492–495.

Kraus, M.J., 1987, Integration of channel and floodplain suites: II. Lateral relations of alluvial paleosols: Journal of Sedimentary Petrology, v. 57, p. 602–612.

Kraus, M.J., 1997, Lower Eocene alluvial paleosols; pedogenic development, stratigraphic relationships, and paleosol/landscape associations: Palaeogeography, Palaeoclimatology, Palaeogeography, v. 129, p. 387–406.

Kus, K., Gastaldo, R.A., Neveling, J., Geissman, J.W., and Looy, C.V., 2017, Calcisols, palynofloras, and rare charcoal from Quaggasfontein, Eastern Cape Province, South Africa: correlations in the Wapadsberg Pass Area and implications for Late Permian climate [Abstract]: Geological Society of America, Abstracts with Program, v. 49, doi:10.1130/abs/2017AM-303520.

Li, J., Gastaldo, R.A., Neveling, J., and Geissman, J.W., 2017, Siltstones across the *Daptocephalus* (*Dicynodon*) and (*Lystrosaurus*) Assemblage Zones, Karoo Basin, South Africa, show no evidence for aridification: Journal of Sedimentary Research, v. 87, p. 653–671.

Lindeque, A., De Wit, M.J., Ryberg, T., Weber, M., and Chevalier, L., 2011, Deep crustal profile across the southern Karoo Basin and Beattie Magnetic Anomaly, South Africa: an integrated interpretation with tectonic implications: South African Journal of Geology, v. 114, p. 265–292.

Machette, M.N., 1985, Calcic soils of southwestern United States, *in* Weide, D.L., and Faber, M.L., eds., Soils and Quaternary Geology of the Southwestern United States: Geological Society of America, Special Paper 203, p. 1–21.

Mack, G.H., James, W.C., and Monger, H.C., 1993, Classification of paleosols: Geological Society of America, Bulletin, v. 105, p. 129–136.

MacLeod, K.G., Smith, R.M.H., Koch, P.L., and Ward, P.D., 2000, Timing of mammal-like-reptile extinctions across the Permian–Triassic boundary in South Africa: Geology, v. 28, p. 227–230.

MacLeod, K.G., Quinton, P.C., and Bassett, D.J., 2017, Warming and increased aridity during the earliest Triassic in the Karoo Basin, South Africa: Geology, v. 45, p. 483–486.

Marriott, S.B., and Wright, V.P., 1993, Palaeosols as indicators of geomorphic stability in two Old Red Sandstone alluvial suites, South Wales: Geological Society of London, Journal, v. 150, p. 1109–1120.

Maruoka, T., Koeberl, C., Hancox, P.J., and Reimold, W.U., 2003, Sulfur geochemistry across a terrestrial Permian–Triassic boundary section in the Karoo Basin, South Africa: Earth and Planetary Science Letters, v. 206, p. 101–117.

McCrea, J.M., 1950, On the isotopic chemistry of carbonates and a paleotemperature scale: The Journal of Chemical Physics, v. 18, p. 849–857, doi:10.1063/1.1747785.

Neveling, J., Gastaldo, R.A., and Geissman, J.W., 2016, Permo-Triassic boundary in the Karoo Basin: Field trip guide Pre-3: Pretoria, Council for Geoscience, 81 p., doi:10.13140/RG.2.2.22414.15683.

Nordt, L., and Driese, S., 2010, New weathering index improves paleorainfall estimates from Vertisols: Geology, v. 38, p. 407–410, doi:10.1130/G30689.1.

Pace, D.W., Gastaldo, R.A., and Neveling, J., 2009, Early Triassic aggradational and degradational landscapes of the Karoo Basin and evidence for climate oscillation following the P-Tr Event: Journal of Sedimentary Research, v. 79, p. 316–331.

Prevec, R., Gastaldo, R.A., Neveling, J., Reid, S.B., and Looy, C.V., 2010, An autochthonous glossoperid flora with Latest Permian palynomorphs from the *Dicynodon* Assemblage Zone of the southern Karoo Basin, South Africa: Palaeogeography, Palaeoclimatology, Palaeoecology, v. 292, p. 381–408, doi:10.1016.

Reeves, C.C., Jr., 1970, Origin, classification, and geologic history of caliche on the southern high plains, Texas and eastern New Mexico: Journal of Geology, v. 78, p. 352–362.

Reeves, C.C., Jr., 1976, Quaternary stratigraphy and geologic history of southern High Plains, Texas and New Mexico: Quaternary Stratigraphy of North America, p. 213–234.

Retallack, G.J., and German-Heins, J., 1994, Evidence from paleosols for the geological antiquity of rain forest: Science, v. 265, p. 499–502.

Retallack, G.J., Smith, R.M.H., and Ward, P.D., 2003, Vertebrate extinction across Permian–Triassic boundary in Karoo Basin, South Africa: Geological Society of America, Bulletin, v. 115, p. 1133–1152.

Rey, K., Amiot, R., Fourel, F., Rigaudier, T., Abdala, F., Day, M.O., Fernandez, V., Fluteau, F., France-Lanord, C., Rubidge, B.S., Smith, R.M, Viglietti, P.A., Zipfel, B., and Lécuyer, C., 2016, Global climate perturbations during the Permo-Triassic mass extinctions recorded by continental tetrapods from South Africa: Gondwana Research, v. 37, p. 384–396.

Roopnarine, P.D., Angielczyk, K.D., Olroyd, S.L., Nesbitt, S.J., Botha-Brink, J., Peecook, B.R., Day, M.O., and Smith, R.M.H., 2017, Comparative ecological dynamics of Permian–Triassic communities from the Karoo, Luangwa, and Ruhuhu basins of southern Africa: Journal of Vertebrate Paleontology, v. 37, supplement 1, p. 254–272.

Rosenau, N.A., Tabor, N.J., Elrick, S.E., and Nelson, W.J., 2013a, Polygenetic history of paleosols in Middle–Upper Pennsylvanian cyclothems of the Illinois basin, USA: part I. Characterization of paleosol types and interpretation of pedogenic processes: Journal of Sedimentary Research, v. 83, p. 606–636.

Rosenau, N.A., Tabor, N.J., Elrick, S.E., and Nelson, W.J., 2013b, Polygenetic history of paleosols in Middle–Upper Pennsylvanian cyclothems of the Illinois basin, USA: part II. Integrating geomorphology, climate, and glacioeustasy: Journal of Sedimentary Research, v. 83, p. 637–668.

Rubidge, B.S., ed., 1995, Biostratigraphy of the Beaufort Group (Karoo Supergroup): Geological Survey of South Africa, Biostratigraphic Series, no. 1, p. 1–46.

Rubidge, B.S., 2005, Re-uniting lost continents: fossil reptiles from the ancient Karoo and their wanderlust: South African Journal of Geology, v. 108, p. 135–172.

Rubidge, B.S., Erwin, D.H., Ramezani, J., Bowring, S.A., and de Klerk, W.J., 2013, High-precision temporal calibration of Late Permian vertebrate biostratigraphy: U-Pb zircon constraints from the Karoo Supergroup, South Africa: Geology, v. 41, p. 363–366.

Semeniuk, V., and Searle, D.J., 1985, Distribution of calcrete in Holocene coastal sands in relation to climate, southwestern Australia: Journal of Sedimentary Petrology, v. 55, p. 86–95.

Sheldon, N.D., 2005, Do red beds indicate paleoclimatic conditions?: A Permian case study, Palaeogeography, Palaeoclimatology, Palaeoecology, v. 228, p. 305–319.

Sheldon, N.D., and Tabor, N.J., 2009, Quantitative paleoenvironmental and paleoclimatic reconstruction using paleosols: Earth Science Reviews, v. 95, p. 1–52.

Shen, S.-Z, Ramezani, J., Chen, J., Cao, C.-Q., Erwin, D.H., Zhang, H., Xiang, L., Schoepfer, S.D., Henderson, C.M., Zheng, Q.-F., Bowring, S.A., Wang, Y., Li, X.-H., Wang, X.-D., Yuan, D.-X., Zhang, Y.-C., Mu, L., Wang, J., and Wu, Y.-S., 2018, A sudden end-Permian mass extinction in South China: Geological Society of America, Bulletin, v. 131, p. 205–223, doi:10.1130/B31909.1.

Smith, R.M., 1990, Alluvial paleosols and pedofacies sequences in the Permian Lower Beaufort of the southwestern Karoo Basin, South Africa: Journal of Sedimentary Petrology, v. 60, p. 258–276.

Smith, R.M.H., 1995, Changing fluvial environments across the Permian–Triassic boundary in the Karoo Basin, South Africa, and possible causes of the extinctions: Palaeogeography, Palaeoclimatology, Palaeoecology, v. 117, p. 81–104.

Smith, R.M.H., and Botha, J., 2005, The recovery of terrestrial vertebrate diversity in the South African Karoo Basin after the end-Permian Extinction: Compte Rendu Palevol, v. 4, p. 555–568.

Smith, R.M.H., and Botha-Brink, J., 2014, Anatomy of a mass extinction: sedimentological and taphonomic evidence for drought-induced-die-offs at the Permo-Triassic boundary in the main Karoo Basin, South Africa: Palaeogeography, Palaeoclimatology, Palaeoecology, v. 396, p. 99–118.

Smith, R.M.H., and Ward, P.D., 2001, Pattern of vertebrate extinctions across an event at the Permian–Triassic boundary in the Karoo Basin of South Africa: Geology, v. 29, p. 1147–1150, doi:10.1130/0091-7613(2001)029<1147:POVEAA>2.0CO;2.

Smith, R.M.H., Eriksson, P.G., and Botha, W.J., 1993, A review of the stratigraphy and sedimentary environments of the Karoo-aged basin of Southern Africa: Journal of African Earth Sciences, v. 16, p. 143–169.

Song, H., Wignall, P.B., Chu, D., Tong, J., Sun, Y., Song, H., He, W., and Tian, L., 2014, Anoxia/high temperature double whammy during the Permian–Triassic marine crisis and its aftermath: Scientific Reports 4, n. 4132, doi:10.1038/srep04132.

Stiles, C.A., Mora, C.I., and Driese, S.G., 2003a, Pedogenic processes and domain boundaries in a Vertisol climosequence: evidence from titanium and zirconium distribution and morphology: Geoderma, v. 116, p. 279–299.

Stiles, C.A., Mora, C.I., Driese, S.G., and Robinson, A.C., 2003b, Distinguishing climate and time in the soil record: mass-balance trends in Vertisols from the Texas coastal prairie: Geology, v. 31, p. 331–334.

Tabor, N.J., and Montañez, I.P., 2004, Morphology and distribution of fossil soils in the Permo-Pennsylvanian Wichita and Bowie Groups, north-central Texas, USA: implica-

tions for western equatorial Pangean palaeoclimate during the icehouse-greenhouse transition: Sedimentology, v. 51, p. 851–884.

Tabor, N.J., and Yapp, C.J., 2005, Coexisting goethite and gibbsite from a high-paleolatitude (55°N) late Paleocene laterite: concentration and $^{13}C/^{12}C$ ratios of occluded and associated organic matter: Geochimica et Cosmochimica Acta, v. 69, p. 5495–5510.

Tabor, N.J., Yapp, C.J., and Montañez, I.P., 2004a, Goethite, calcite, and organic matter from Permian and Triassic soils: carbon isotopes and CO_2 concentrations: Geochimica et Cosmochimica Acta, v. 68, p. 1503–1517.

Tabor, N.J., Montañez, I.P., Zierenberg, R., and Currie, B.S., 2004b, Mineralogical and geochemical evolution of a basalt-hosted fossil soil (Late Triassic Ischigualasto Formation, northwest Argentina): potential for paleoenvironmental reconstruction: Geological Society of America, Bulletin, v. 116, p. 1280–1293.

Tabor, N.J., Montañez, I.P., Steiner, M., and Schwindt, D., 2007, The $\delta^{13}C$ values of Permo–Triassic carbonates from South Africa reflect a stinking, sulfurous swamp, not atmospheric conditions: Palaeogeography, Palaeoclimatology, Palaeoecology, v. 225, p. 370–381.

Tabor, N., Meyers, T.S., and Michel, L.A., 2017, Sedimentologist's guide for recognition, description, and classification of paleosols, *in* Ziegler, K., and Parker, W., eds., Terrestrial Depositional Systems: Elsevier, p. 165–208, doi:10.1016/B978-0-12-803243-5.00004-2.

Thomas, S.G., Tabor, N.J., Yang, W., Myers, T.S., Yang, Y., and Wang, D., 2011, Palaeosol stratigraphy across the Permian–Triassic boundary, Bogda Mountains, NW China: implications for palaeoenvironmental transition through Earth's largest mass extinction: Palaeogeography, Palaeoclimatology, Palaeoecology, v. 308, p. 41–64.

Viglietti, P.A., Smith, R.M.H., Angielczyk, K.D., Kammerer, C.F., Fröbisch, J., and Rubidge, B.S., 2016, The *Daptocephalus* Assemblage Zone (Lopingian), South Africa: a proposed biostratigraphy based on a new compilation of stratigraphic ranges: Journal of African Earth Sciences, v. 113, p. 153–164.

Viglietti, P.A., Rubidge, B.S., and Smith, R.M.H., 2017, New Late Permian tectonic model for South Africa's Karoo Basin: foreland tectonics and climate change before the end-Permian crisis: Scientific Reports, v. 7, doi:10.1038/s41598-017-09853-3.

Viglietti, P.A., Smith, R.M.H., and Rubidge, B.S., 2018, Changing palaeoenvironments and tetrapod populations in the *Daptocephalus* Assemblage Zone (Karoo Basin, South Africa) indicate early onset of the Permo-Triassic mass extinction: Journal of African Earth Sciences, v. 138, p. 102–111.

Vitali, F., Longstaffe, F.J., McCarthy, P.J., Plint, G.A., Caldwell, W., and Glen, E., 2002, Stable isotopic investigation of clay minerals and pedogenesis in an interfluve paleosol from the Cenomanian Dunvegan Formation, N.E. British Columbia, Canada: Chemical Geology, v. 192, p. 269–287.

Ward, P.D., Montgomery, D.R., and Smith, R.M.H., 2000, Altered river morphology in South Africa related to the Permian–Triassic extinction: Science, v. 289, p. 1740–1743, doi:10.1126/science.289.5485.1740.

Ward, P.D., Botha, J., Buick, R., DeKock, M.O., Erwin, D.H., Garrison, G., Kirschvink, J., and Smith, R.M.H., 2005, Abrupt and gradual extinction among Late Permian land vertebrates in the Karoo Basin, South Africa: Science, v. 307, p. 709–714, doi:10.1126/science.1107068.

Weitkamp, W.A., Graham, R.C., Anderson, M.A., and Amrhein, C., 1996, Pedogenesis of a vernal pool Entisol–Alfisol–Vertisol catena in southern California: Soil Science Society of America, Journal, v. 60, p. 316–323.

Wright, V.P., and Wilson, R.C.L., 1987, A Terra Rossa-like paleosol complex from the Upper Jurassic of Portugal: Sedimentology, v. 34, p. 259–273.

Yapp, C.J., 2004, $Fe(CO_3)OH$ in goethite from a mid-latitude North American Oxisol: estimate of atmospheric CO_2 concentration in the Early Eocene "Climatic Optimum": Geochimica et Cosmochimica Acta, v. 68, p. 935–947.

Received 2 December 2019; accepted 13 January 2020.